J. Fluid Mech. (1986), *vol.* 169, *pp.* 535–564
Printed in Great Britain

Mechanisms of impulsive pressure generation and damage pit formation by bubble collapse

By Y. TOMITA AND A. SHIMA
Institute of High Speed Mechanics, Tohoku University, Sendai, Japan

(Received 28 August 1985)

A detailed experimental study has been made to clarify the mechanism of impulsive pressure generation from a single bubble collapsing in a static fluid – this is the most essential and important research task concerned with cavitation damage. First, the general feature of impulsive pressure generation is discussed, and then the impulsive pressure directly contributing to damage is investigated by various means. As a result, it is found that the impulsive pressure causing plastic deformation of material is closely related, directly or indirectly, to the behaviour of a liquid jet. Further more, it is demonstrated that the interaction of a tiny bubble with a shock wave or a pressure wave must be an important effect in producing a local high pressure which causes damage to material. The damage pit caused by the bubble–shock-wave interaction essentially results from the impact pressure from a liquid microjet.

1. Introduction

It is generally understood that cavitation damage is predominantly caused by impulsive pressure produced from collapsing bubbles (Knapp 1955). The cumulative effect of this pressure on a material surface is deformation and finally particle removal. Much research has been done in connection with the generation of this impulsive pressure.

Rayleigh (1917) theoretically pointed out a local high pressure produced in the final stage of bubble collapse. The essential consideration was supported by Shutler & Mesler (1965), who performed an experiment on spark-induced bubbles and concluded that the damage pattern must be caused by pressure pulses resulting from bubble collapse. In the case of a no-empty bubble interior the gas pressure inside a bubble rapidly increases in the final stage of collapse and finally overcomes the liquid inertia. Subsequently, a shock wave radiates into the liquid owing to rebound of the bubble. Several investigations (Hickling & Plesset 1964; Fujikawa & Akamatsu 1978, 1980) have produced evidence that this shock-wave pressure is an important factor contributing to cavitation damage.

Another important cause of damage is revealed as a result of non-spherical collapse of a bubble. The most probable causes of non-spherical symmetric flow in actual situations are the presence of boundaries and pressure gradients, including interaction of a bubble with a shock wave. When an initially spherical bubble collapses near a boundary, its surface gradually departs from spherical symmetry. The bubble surface is deformed according to the degree of non-sphericity in the flow field around the bubble. In suitable conditions the deformation will result in the generation of a liquid jet directed towards the solid boundary. Since Kornfeld & Suvorov (1944) pointed out that the liquid microjet is a dominant factor in cavitation damage, the jet behaviour has been studied by numerous investigators (Naudé & Ellis 1961;

Benjamin & Ellis 1966; Gibson 1968; Plesset & Chapman 1971; Kling & Hammitt 1972; Lauterborn & Bolle 1975). Immediately after jet impact on a solid boundary, an impulsive pressure with a very short duration is produced and followed by a pressure fluctuation due to the stagnation pressure. Since the water-hammer pressure corresponding to an impact velocity of several hundred metres per second is larger than the yield point of common metal materials, the abovementioned investigators conclude that liquid-jet impact is an effective factor contributing to cavitation damage. However, it may be relevant that, as found numerically by Plesset & Chapman (1971), Huang, Hammitt and Yang (1973) and Hwang & Hammitt (1977), the duration of the impulsive pressure due to liquid-jet impact is very short. This suggests that knowledge of the yield strength of a material for an extremely short loading duration is needed to make clear the cause of damage. In fact it is true that common metal materials can be easily eroded by impingement of a water jet with sufficiently large energy (Bowden & Brunton 1961). In contrast, for the case of a liquid jet formed inside a bubble, a higher velocity is required to cause plastic deformation on the material surface owing to its minute size. The possibility of such a high-speed liquid jet was theoretically predicted by Tulin (1969), who showed that when a weak shock impinges on a cavity, an ultrajet having a velocity greater than half the velocity of sound in the liquid may be induced within it. His suggestion shows the importance of the interaction between a bubble and a shock wave in actual cavitating flow. Until now there has been no experimental evidence associated with the existence of ultrajet; however, it is of great significance to study the interaction of a bubble with either a shock wave or a pressure wave from the point of view of the local generation of high pressure. Hansson & Mørch (1980) adapted this interaction problem for the dynamics of cavity clusters and showed the simultaneous collapse of a cluster of cavities. Furthermore, Tomita, Shima & Takahashi (1983), Tomita, Shima & Ohno (1984), Tomita, Shima & Sugiu (1986), Shima, Tomita & Takahashi (1984) demonstrated an increase in damage due to bubble–shock-wave interaction.

Although much work has been done in order to explain impulsive pressure generation in connection with cavitation damage, the detailed mechanism is still unknown because the phenomenon is too rapid and small to observe. From the observation of material surfaces exposed to cavitation, on the other hand, it has been found that this does seem to cause damage (Efimov *et al.* 1976). However, there is no actual evidence for a direct causal test between cavitation and material damage, even in the simplest case like a single bubble in a static fluid.

The present paper describes an experimental investigation into the mechanism of impulsive pressure generation and damage-pit formation from bubble collapse. First, general features of impulsive pressure generation from spark-induced bubble collapse are examined, and the cause of the damage produced on an indium specimen is clarified. Next, as one of the most probable mechanisms for causing damage, bubble–shock-wave interaction is studied. As a result, it is found that the behaviour of a liquid jet is closely related, directly or indirectly, to the generation of impulsive pressure, which contributes to damage-pit formation. The damage pattern resulting from spark-induced bubble collapse may be caused by the local high pressure generated at the collision between the contracting bubble surface and the radial flow following liquid-jet impact on a solid boundary. The fact that extremely short pressure pulses successively impinge on the material surface is of significance in the deformation of the material. The damage pit caused by the bubble–shock-wave interaction results from the impact pressure from a liquid microjet.

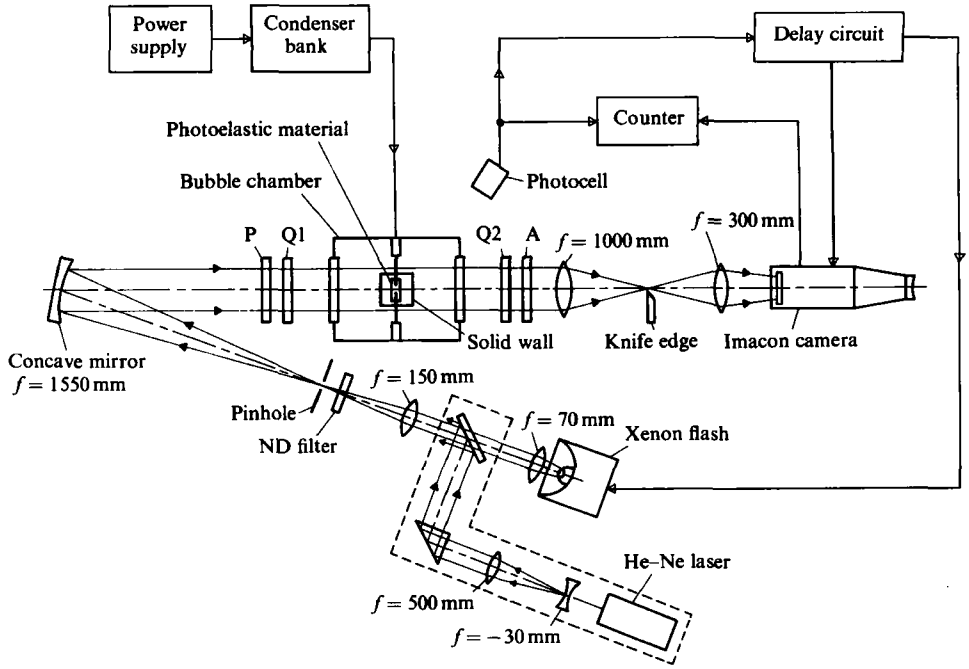

FIGURE 1. Schematic diagram of the experimental setup: P, polarizer, A, analyser; Q1 and Q2 are $\frac{1}{4}\lambda$ plates, where λ is the wavelength of light.

2. Experiment

2.1. *Experimental equipment and methods*

A schematic diagram of the experimental setup is shown in figure 1. A 240 mm × 240 mm × 300 mm stainless-steel bubble chamber with 100 mm diameter optical windows was used and filled with tap water at room temperature. At the centre of the chamber two tungsten electrodes of 0.3 mm diameter were placed facing each other. A solid boundary was set vertically above or sometimes below the electrodes. Three kinds of solid boundaries were employed in the present experiment: (i) one mounted with a pressure transducer; (ii) one made of photoelastic material; (iii) one made of soft material.

(i) The transducer (Swiss Kistler 603B) had a diameter of 5.55 mm, a resonant frequency of 400 kHz with a rise time of about 1 μs to allow step changes in pressure and was capable of measuring pressures up to 25 MPa with a resolution of 0.5 kPa. The results obtained from the transducer were only qualitative, however, because of its non-uniform spatial sensitivity (Tomita *et al.* 1984).

(ii) An epoxy resin with thickness of 6 mm was used as a photoelestic material and placed between two phosphorbronze plates with thicknesses of 0.5 mm to make a flat boundary. The photoelastic method is very useful for observing a local stress state in a solid.

(iii) The third method for studying impulsive pressure employs a soft material as a solid boundary. Indium was used here and was cast into a brass container with outer diameter of 9.9 mm. It was initially confirmed that a damage pit caused by bubble collapse can be distinguished from a melting mark caused by underwater spark discharge.

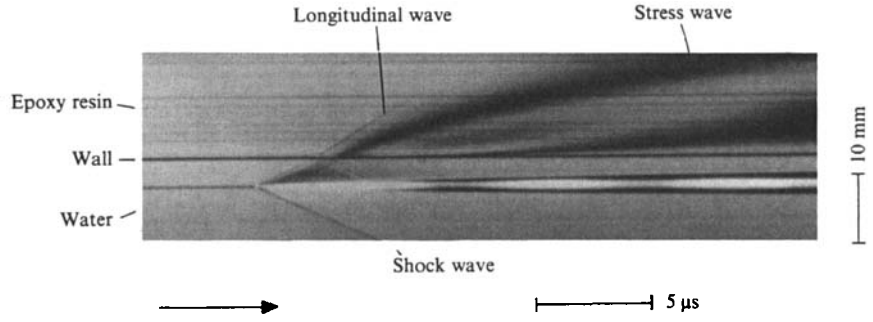

FIGURE 2. Propagation of a shock wave and stress waves in epoxy resin; photoelastic sensitivity $\alpha = 5.2$ mm/kg.

The optical system was as follows. As shown in figure 1, a typical photoelastic system was combined with a schlieren system allowing simultaneous observations of both a shock wave in water and a stress wave in solid. The phenomena photographed using an Imacon high-speed camera (John Hadland 790), with a Xenon microflash with light-pulse width of about 200 μs as a light source. This generated a light intensity sufficient for the photography. Stress fringes of higher order lacked clarity owing to the light source not being monocromatic light; however, the lower-order stress fringes were detectable. Thus this method enabled study of the temporal correlation between shock-wave impact and a stress-fringe initiation. For synchronization with the phenomena, a spark light radiated at the instant of underwater spark discharge was used. An output signal from a photocell was supplied to the camera through a delay circuit. On the other hand, the behaviour of the liquid jet formed within a bubble was observed using a different optical system from that in figure 1 in which back lighting with a diffuser was used for visualizing the bubble interior.

For examining bubble–shock-wave interaction a shock wave generated at the instant of underwater spark discharge caused an air bubble to collapse, and the amplitude of the shock wave as it interacted with the bubble was monitored by means of a pressure transducer mounted flush to the lower solid boundary.

2.2. *Dynamic responses of photoelastic material*

The observation of the impulsive stress caused by bubble collapse requires knowledge of the dynamic responses of a photoelastic material. Three kinds of epoxy plates with different photoelastic sensitivities α (= 1.0, 5.2 and 7.3 mm/kg) were taken here as model materials. On this occasion shock-wave pressure produced at the instant of the spark discharge was employed as the impulsive force acting on the materials.

Figure 2 shows an example of photographs taken in the streaking mode. It clearly shows the dynamic response of the epoxy resin to an impulsive force with waves propagating in water as well as in solid. The transmitted component from the primary shock wave propagates into the epoxy resin as a longitudinal wave with velocity c_e, which can be readily obtained as the gradient on the photograph. When the state of stress in the solid is increased owing to the longitudinal wave and reaches the threshold value for generation of the stress fringe of minimum order (i.e. $\frac{1}{2}$th order), an isochromatic fringe becomes visible. To obtain dynamic responses of the photoelastic material, the lower solid wall with the pressure transducer was mounted at the same distance from the source of the shock wave as the upper surface.

Figures 3(*a–c*) show the results for the retardation time T_d, the initial fringe

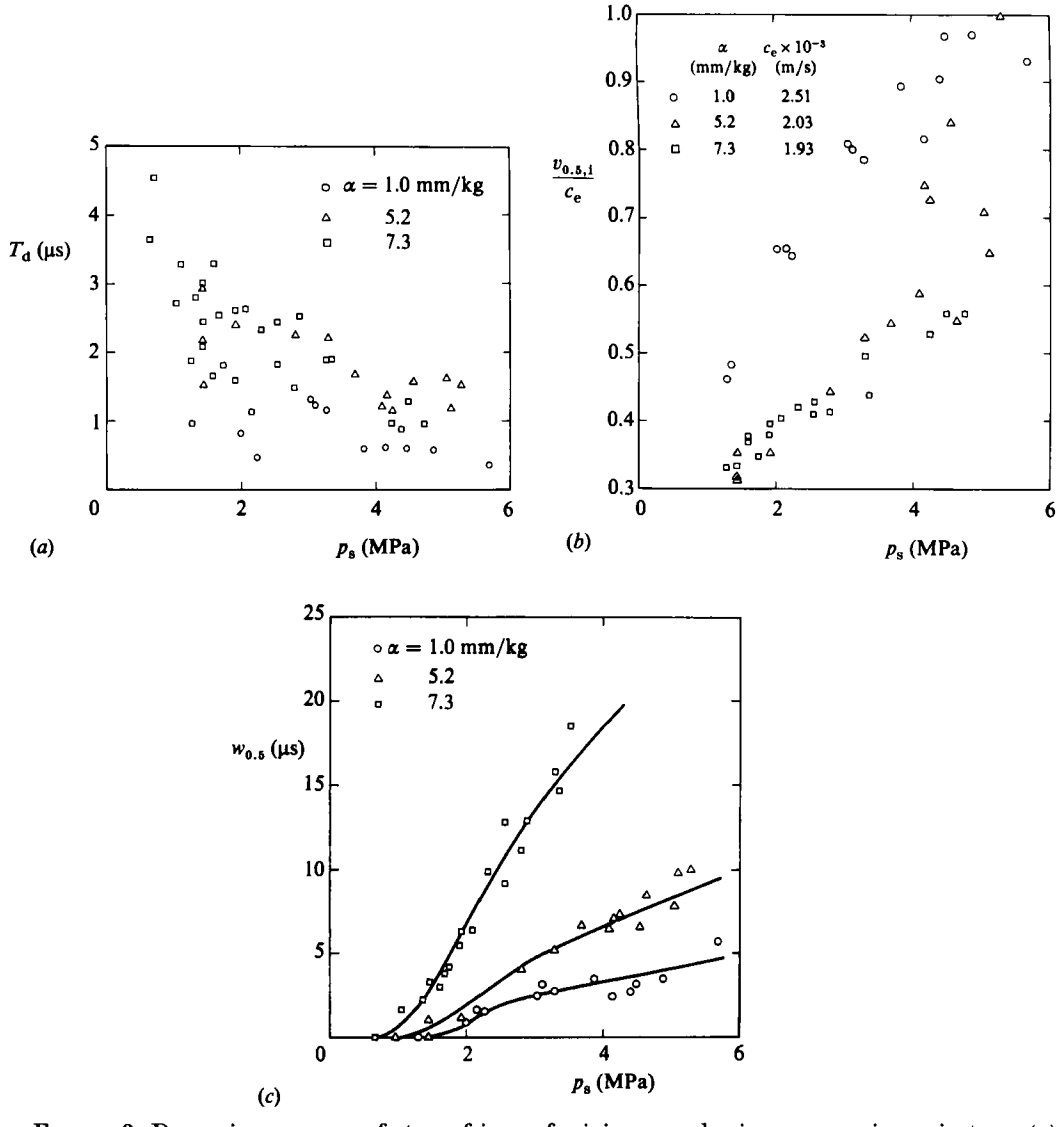

FIGURE 3. Dynamic responses of stress fringe of minimum order in epoxy resin against p_s: (*a*) retardation time T_d; (*b*) initial propagation velocity $v_{0.5,1}$; (*c*) duration of stress at the epoxy surface, $w_{0.5}$.

propagation velocity $v_{0.5,1}$ and the stress duration at the epoxy surface, $w_{0.5}$, for various shock-wave amplitudes p_s. The retardation time is defined as the time difference from the impact time of an incident shock wave on the surface to the initiation time of a fringe. Figure 3(*a*) indicates that larger p_s results in smaller T_d. In this situation, the fringe tends to follow just behind a longitudinal wave. The impact times of multiple impulsive pressures should, therefore, be carefully determined, since the velocity $v_{0.5,1}$ depends on the applied pressure (figure 3*b*). For the duration $w_{0.5}$ it is obvious that it is longer for higher α.

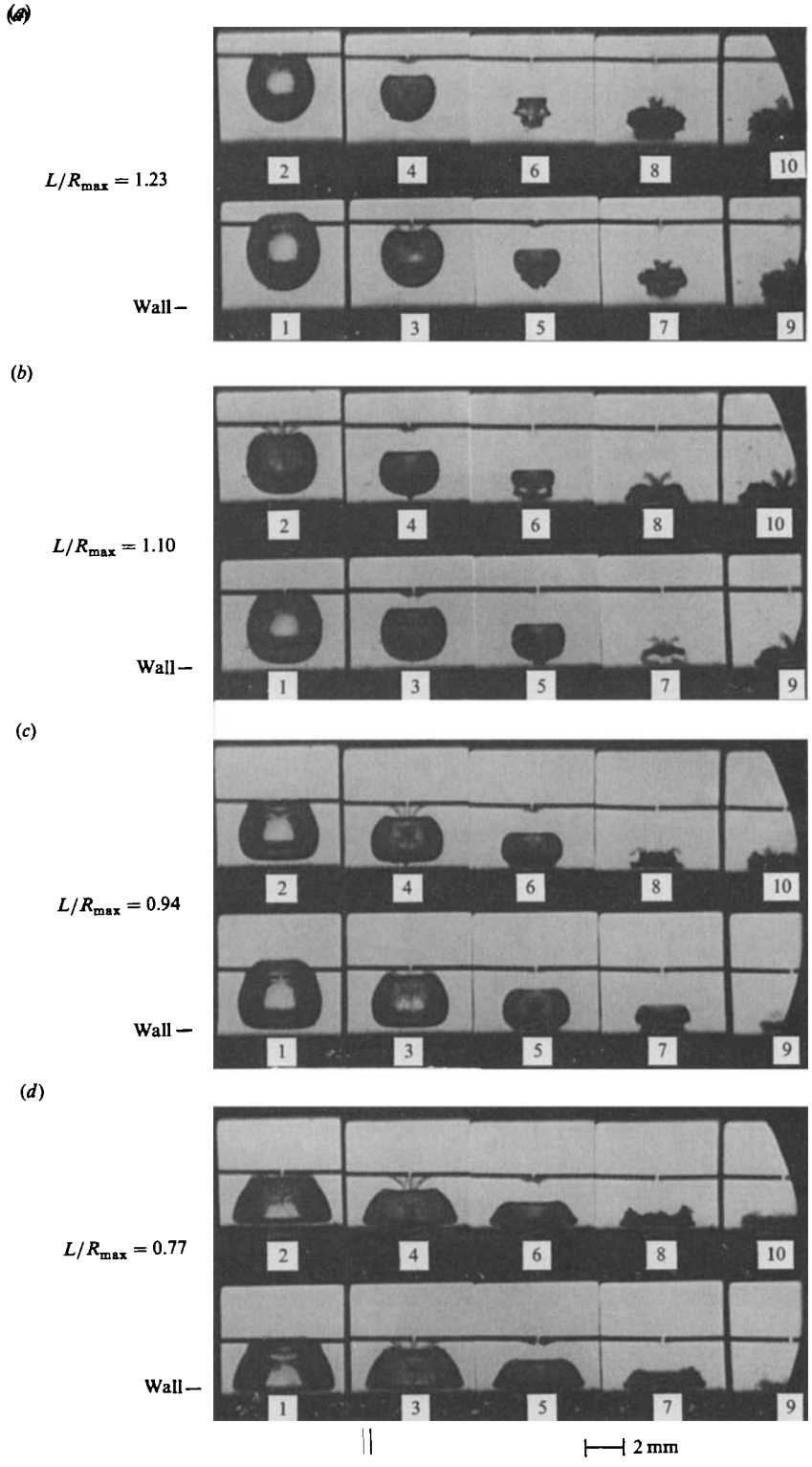

FIGURE 4. First collapse of spark-induced bubbles for various L/R_{max}; the maximum bubble radius $R_{max} = 3.5$ mm, frame interval 10 μs, exposure 2 μs.

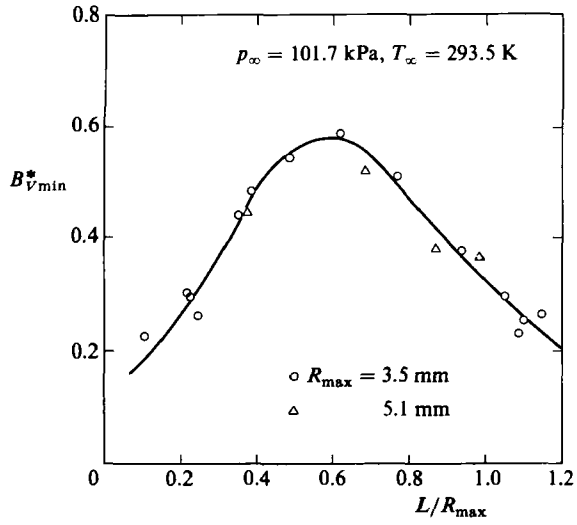

FIGURE 5. Variation with dimensionless distance $L/R_{\max}$ of the dimensionless bubble base diameter $B^*_{V\,\min}$ at the minimum volume of a bubble.

3. Results and discussion

3.1. *Impulsive pressure generation and damage pattern from spark-induced bubble collapse*

In this section, first the collapse process of a single spark-induced bubble near a boundary is described, and secondly the general features of impulsive pressure generation are systematically studied. Finally the cause of damage pattern produced on an indium specimen is clarified.

3.1.1. *Collapse of a bubble near a boundary and formation of a liquid jet*

One of the most pronounced features of bubble collapse near a boundary is formation of a liquid jet within the bubble. Naturally, the behaviour of this jet is affected by the degree of the proximity of the bubble to a boundary. Some aspects of the initial collapse of bubbles generated at various positions were observed using a high-speed camera. Figure 4 shows selected photographs taken with a framing rate of 100000 frames/s, where the maximum bubble radius $R_{\max}$ is fixed as 3.5 mm and L is the distance from the spark gap to the solid boundary. Where a bubble is very close to the boundary ($L/R_{\max} = 1.10$), it migrates toward that boundary owing to translational motion rapidly induced in the final stage of collapse. At the same time, a liquid jet developing opposite to the solid boundary penetrates the lower surface of the bubble and collides with the boundary. Subsequently the jet turns outwards as a radial flow. When a bubble attaches to the boundary at its maximum expansion, the radial flow will collide with the contracting bubble surface touching the solid boundary. Figure 5 shows the dimensionless base diameter $B^*_{V\,\min}$ ($= B_{V\,\min}/2R_{\max}$) of a bubble attached to a solid boundary at a virtual minimum bubble volume versus the dimensionless distance $L/R_{\max}$. The data were taken for both $R_{\max} = 3.5$ mm and 5.1 mm. The virtual volume is the bubble volume ignoring the volume loss resulting from liquid-jet formation. It can be seen that $B^*_{V\,\min}$ is significantly affected by radial flow along the solid surface. As seen in figure 5, the $B^*_{V\,\min}$ versus $L/R_{\max}$ curve

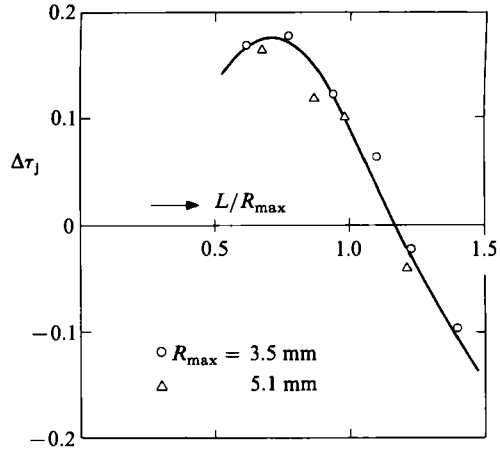

FIGURE 6. Impact time of a liquid jet on a solid boundary.

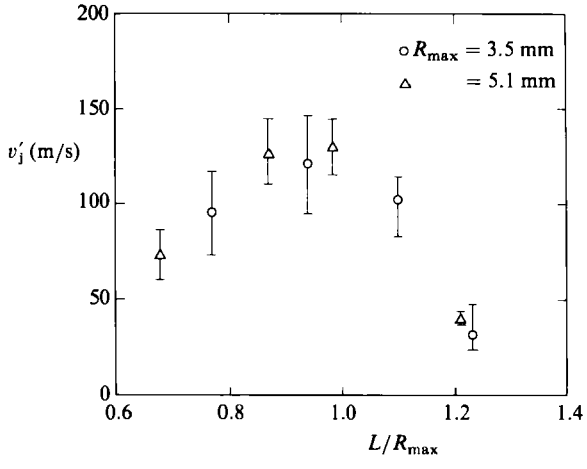

FIGURE 7. Impact velocity of a liquid jet.

possesses a maximum at a certain value of L/R_{max} because the outward radial flow suppresses the inward motion of the bubble surface.

Figure 6 shows the dimensionless relationship between $\Delta\tau_j$ and L/R_{max}. Here

$$\Delta\tau_j = \frac{\Delta T_j}{R_{max}}\left(\frac{p_\infty - p_v}{\rho_\infty}\right)^{\frac{1}{2}}, \tag{1}$$

where ΔT_j is difference between the impact time of the liquid jet on the solid boundary and the time at virtual minimum bubble volume; p_∞ is the pressure in the liquid at infinity, p_v the vapour pressure inside the bubble and ρ_∞ the liquid density. In figure 6 the maximum measuring error was estimated to be about 10 μs. $\Delta\tau_j > 0$ implies that a liquid jet hits the solid boundary before the bubble reaches its minimum volume. Bubbles in the region $L/R_{max} \lesssim 1.2$ satisfy this condition. In particular, for an attached bubble at $L/R_{max} \approx 0.6$–0.7, a liquid jet is formed at the earliest stage

of collapse and impacts on the solid boundary at $\Delta\tau_j \approx 0.17$. On the other hand, for smaller $L/R_{\max}$ it was difficult to obtain data on $\Delta\tau_j$ because of the narrower view into the bubble. However, it can be estimated that $\Delta\tau_j$ decreases monotonically, since it was confirmed that a liquid jet cannot appear inside the bubble until 4 μs before its minimum volume when a bubble is located at $L/R_{\max} = 0.089$.

Figure 7 shows the relationship between the virtual impact velocity of a liquid jet, v_j', and the dimensionless distance $L/R_{\max}$. The prime indicates that the impact velocity was directly measured from a photograph without any correction. The actual impact velocity must be different from the virtual one owing to optical refraction effects. The magnification m of an object located at the centre of a hemispherical bubble, for example, can be expressed as follows by using formulae for refraction in homogeneous media:

$$m = \frac{3}{4}\left[1 + K\rho_0\left(\frac{R_0}{R}\right)^3\right], \tag{2}$$

where K is the Gladstone–Dale constant, R_0 is the initial equivalent radius of a spherical bubble having the same volume as the bubble under consideration, and ρ_0 is the initial gas density inside the bubble. Equation (2) gives $m = 0.75$ for a bubble in an initial equilibrium state. In the final stage of bubble collapse, the magnification associated with the behaviour of a liquid jet will tend to be around unity owing both to the smaller curvature of the bubble surface and the increase in gas density. Keeping in mind the refraction effect, return to figure 7. The average maximum impact velocity obtained from ten data points reaches about 130 m/s at $L/R_{\max} \approx 0.9$–1.0, whereas it is about 50 m/s at $L/R_{\max} \approx 0.6$.

It is well known that the water-hammer pressure induced by an impacting liquid jet can be expressed as

$$p_{\mathrm{WH}} = \rho_\infty c_\infty v_j. \tag{3}$$

In this case the pressure duration is

$$t_{\mathrm{WH}} \approx \frac{d_j}{2c_\infty}, \tag{4}$$

where c_∞ is the velocity of sound in the liquid and d_j the diameter of the liquid jet. For instance, we obtain $p_{\mathrm{WH}} = 150$ MPa when $v_j = 100$ m/s. Plesset & Chapman (1971) indicated that the jet diameter is about one tenth of the initial bubble diameter. In the case of a bubble with an initial radius $R_0 = 1$ mm, for instance, this gives $t_{\mathrm{WH}} \simeq 10^{-7}$ s. In fact the value of 150 MPa is larger than the yield points of several common metals. In this situation, however, the dynamic strength at the yield point should be considered because of the extremely short pressure duration which is of the order of 10^{-7} s. This problem will be discussed below. In figure 7 it was found that the impact velocities at specified $L/R_{\max}$ are in good agreement with previous results (Gibson 1968; Kling & Hammitt 1972; Plesset & Chapman 1971). For $L/R_{\max} < 0.6$, v_j' may increase with decreasing $L/R_{\max}$, which can be readily estimated from figure 5.

3.1.2. *Impulsive pressure generation by bubble collapse*

In the preceding subsection, the motion of a bubble was observed and, in particular, the behaviour of a liquid jet was studied. Next the general features of the impulsive pressures generated by a bubble collapsing near a solid boundary are discussed with reference to results obtained by pressure-transducer and photoelastic methods.

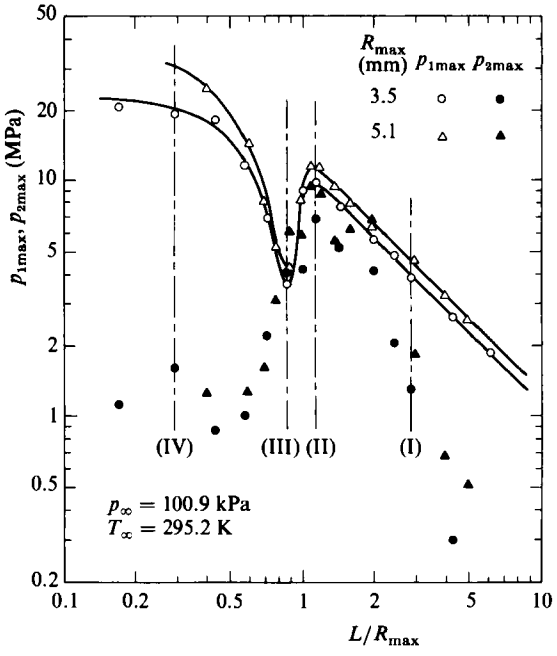

FIGURE 8. Relationship between the maximum impulsive pressures at both the first and second collapses of a bubble, p_{1max} and p_{2max}, and the dimensionless distance L/R_{max}.

Figure 8 shows the maximum impulsive pressures $p_{N\,max}$, measured with a pressure transducer at both the first and second collapses of a bubble, versus dimensionless distance L/R_{max}, where bubbles with radii $R_{max} = 3.5$ and 5.1 mm were used. The p_{1max} versus L/R_{max} curves are similar to previous results (Shima *et al.* 1983, 1984). The region where p_{1max} quickly decreases with decreasing L/R_{max} just corresponds to the region giving the maximum impact velocity of a liquid jet, as seen in figure 7. On the other hand, the maximum values in $p_{2\,max}$ are present at $L/R_{max} \approx 1.1$. This therefore means that when a bubble collapses in the neighbourhood of a solid boundary, the boundary must be hit by the impulsive pressures produced not only at the first but also at the second collapse of the bubble.

In order to discuss the results in figure 8 in detail it is useful to show schlieren photographs. Figure 9 shows almost spherical shock waves emitted from bubbles (*a*) far from and (*b*) relatively close to a solid boundary. Figures 10–12 show streak schlieren photographs and pressure histories at the first collapse of a bubble for the dimensionless distances L/R_{max} specified in figure 8. In these figures the point B corresponds to the generation of a shock wave coming from the rebound of an original bubble. Shock waves can be seen wherever a bubble collapses, as shown by previous studies (Fujikawa & Akamatsu 1978; Shima *et al.* 1981). In particular, multiple weak shock waves generated immediately before the point B should be noted, because the pressure rise on the p versus t curve in figure 12 almost corresponds to the generation of these shock waves.

Now we return to figure 8. As mentioned before, the characteristics of the impulsive pressure may be influenced by the behaviour of a liquid jet. First, the case $\Delta T_j > 0$, that is $L/R_{max} \gtrsim 1.2$, is considered. In this case the shock wave impacts before the liquid jet at the first collapse of a bubble. When a bubble is located closer to the

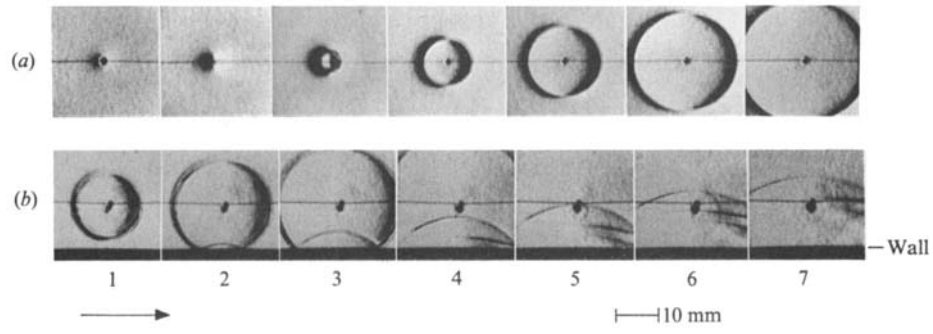

FIGURE 9. Shock waves emitted from bubbles (*a*) far from ($L/R_{\max} \to \infty$) and (*b*) close to a solid boundary ($L/R_{\max} = 2.8$); $R_{\max} = 3.5$ mm, frame interval 2 μs, exposure 0.4 μs.

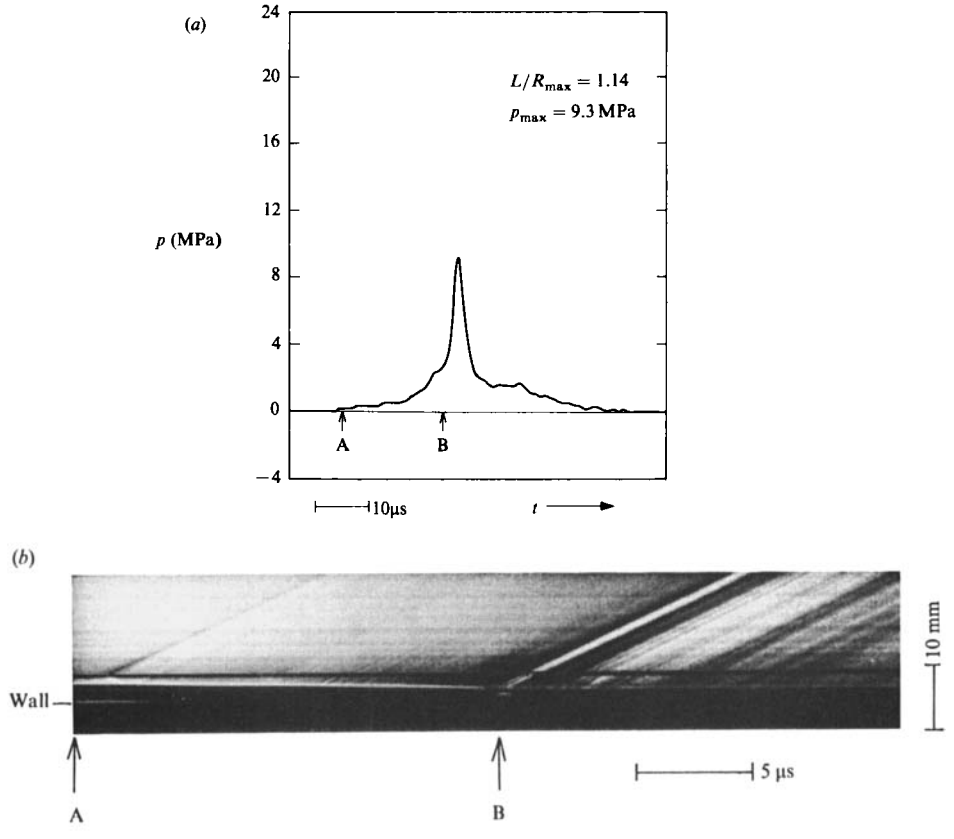

FIGURE 10. Simultaneous records on (*a*) a pressure history and (*b*) a streak schlieren photograph of a portion of the first collapse; $R_{\max} = 3.5$ mm, $L/R_{\max} = 1.14$.

boundary, a lower pressure occurs because of the decrease in sphericity of the bubble collapse. On the other hand, translational motion is induced and rapidly accelerated in the final stage of bubble collapse; subsequently the bubble migrates towards the boundary. For $L/R_{\max} = 2$ at the minimum bubble volume, the bubble centre, which is the origin of the shock wave, is moved towards the boundary from the original position by about 20 % (Shima *et al.* 1984). As a result, $p_{1\max}$ decreases inversely with

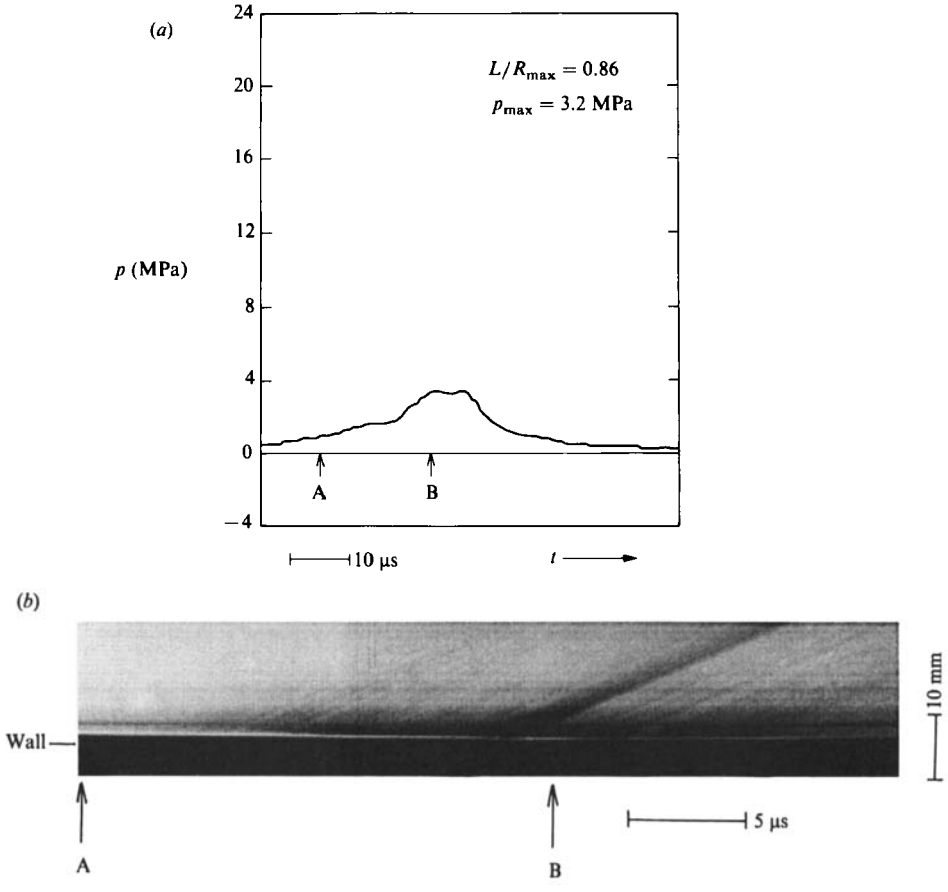

FIGURE 11. Simultaneous records on (*a*) a pressure history and (*b*) a streak schlieren photograph of a portion of the first collapse; $R_{max} = 3.5$ mm, $L/R_{max} = 0.86$.

increasing L/R_{max} from a position close to the solid boundary. When the p_{1max} versus L/R_{max} curve is extrapolated along an L^{-1} curve to 0.2 mm (which is equivalent to a final minimum radius of the bubble with $R_{max} = 3.5$ mm at $L \to \infty$), we can estimate the maximum bubble-wall pressure p_{max} to be about 200 MPa, whereas adiabatic compression of a bubble with the same radius results in $p_{max} \approx 400$ MPa.

Next, the case of $\Delta T_j' > 0$, that is $L/R_{max} \lesssim 1.2$, is considered. In this case the liquid-jet impact precedes the shock-wave one; the impulsive pressure is therefore influenced by a complicated flow following the liquid-jet impact. Liquid flows radially outward along the solid surface taking some gas or vapour with it, and collides with the contracting bubble surface. This liquid–liquid impact results in the creation of tiny new bubbles from the disintegration of the gas–liquid interface. These induced bubbles are exposed to a high-pressure field, which develops in the liquid near the bubble surface in the final stage of the original bubble collapse; they are subjected to pressure waves resulting from the liquid–liquid impact. If the pressure field is fully developed, the bubbles may collapse rapidly, and consequently impulsive forces will locally impinge on the solid boundary. The development of the high-pressure field depends on the period of collision of the radial liquid flow with the contracting bubble surface. When the collision occurs near the point of minimum bubble volume, more

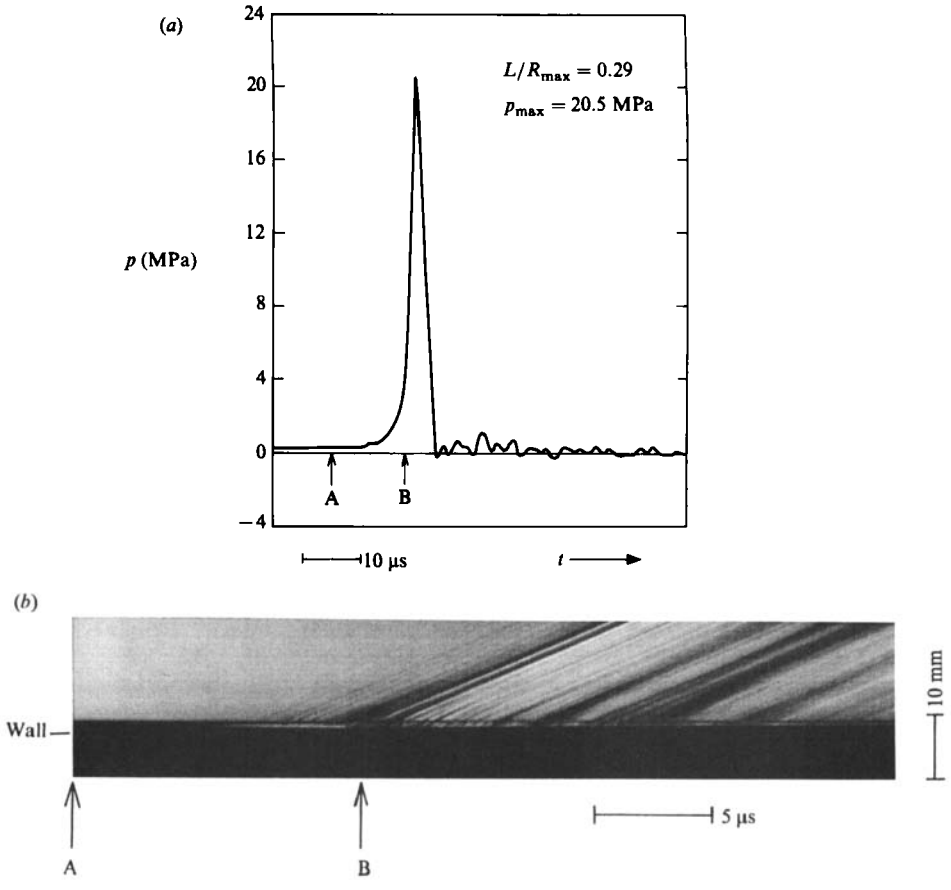

FIGURE 12. Simultaneous records on (*a*) a pressure history and (*b*) a streak schlieren photograph of a portion of the first collapse; $R_{max} = 3.5$ mm, $L/R_{max} = 0.29$.

rapid bubble collapse may take place. Supposing the velocity of a radial liquid flow to be the same as that of a liquid-jet impact and estimating the collision period from figures 5–7, we find the earliest collision period to be at $L/R_{max} \approx 0.6$–1. In this region, therefore, the pressure field is low enough for only a weak bubble collapse to occur. For the region $L/R_{max} < 0.6$, p_{1max} increases with decreasing L/R_{max}, since bubbles collapse more rapidly owing to smaller initial perturbations from the hemispherical shape, as shown in figure 12.

To obtain both spatial and temporal information about impulsive pressure, the photoelasticity technique was used. First the temporal characteristic was examined. Figure 13 shows photoelastic schlieren photographs taken in the streaking mode at the first collapse of a bubble whose maximum radius R_{max} is 3.5 mm. If a bubble collapses relatively far from a boundary (figure 13*a*) the stress fringe of minimum order becomes visible just after impact of a shock wave on the boundary. Furthermore, when a bubble is closer or attached to the boundary, the fringe can be clearly seen prior to the occurrence of the main shock wave. The results obtained from these photographs are plotted in figures 14 and 15. Figure 14 shows a comparison of $\Delta T_{0.5}$ with ΔT_j versus L/R_{max}. Here $\Delta T_{0.5}$ is the difference between the times of fringe initiation and minimum bubble volume. From this figure it is found that ΔT_j is greater

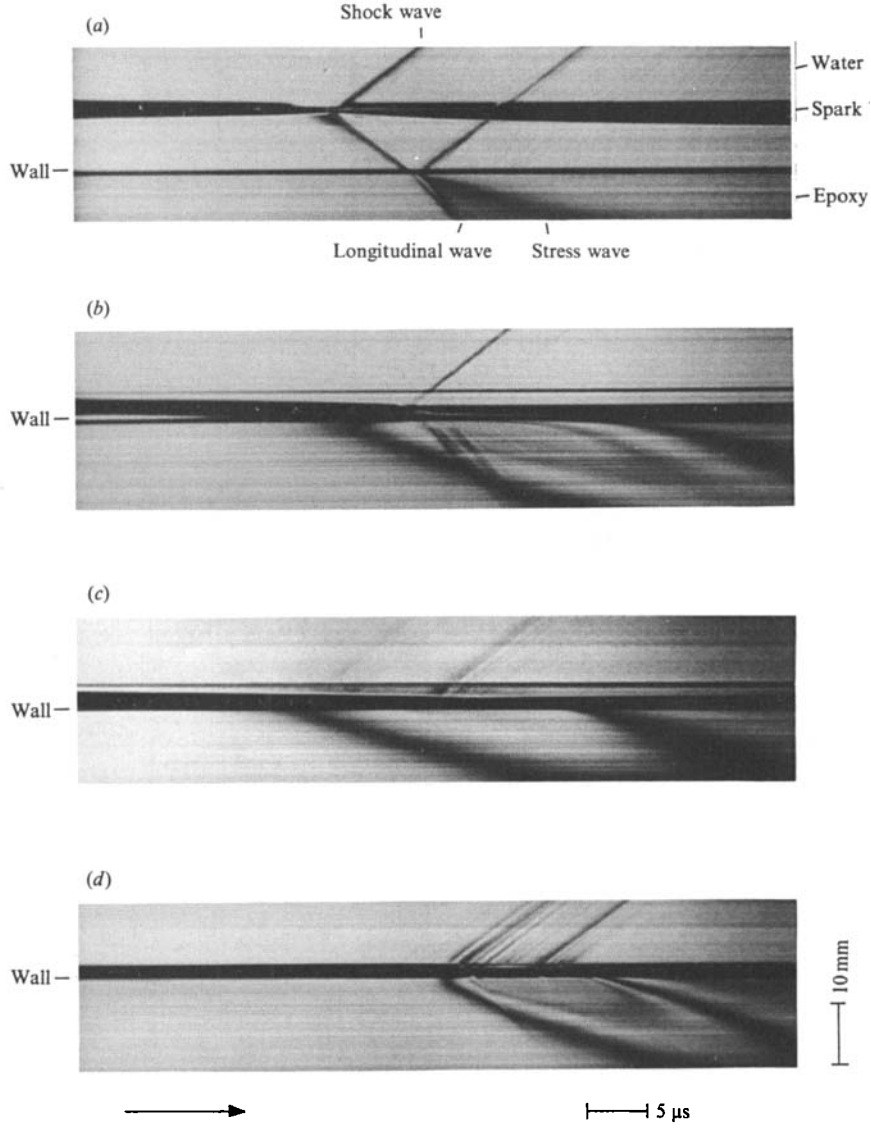

FIGURE 13. Photoelastic photographs taken in the streaking mode at the first collapse of bubbles for various distances L/R_{max}; $R_{max} = 3.5$ mm, $\alpha = 5.2$ mm/kg: (*a*) $L/R_{max} = 2.92$; (*b*) 1.21; (*c*) 0.86; (*d*) 0.29.

than $\Delta T_{0.5}$ in a wide range of L/R_{max}. In general, $\Delta T_{0.5}$ depends on the properties of the photoelastic material as well as the characteristics of the applied pressure. The higher the sensitivity α is, the larger $\Delta T_{0.5}$ is, and *vice versa*. For a bubble located extremely near a solid boundary, it is difficult to distinguish $\Delta T_{0.5}$ from ΔT_j. In other words, the initiation of a stress fringe does not always correspond to the impact time of either a liquid jet or a shock wave radiated at the rebound of the original bubble. If a liquid jet with sufficiently large energy impacts on the surface of a photoelastic material, however, the lowest stress fringe can be detected. Figure 16 shows a typical example, where $R_{max} = 5.1$ mm and $L/R_{max} = 0.68$. The fringe can be seen in the first frame. Since the average first-collapse time of a bubble with the same radius is

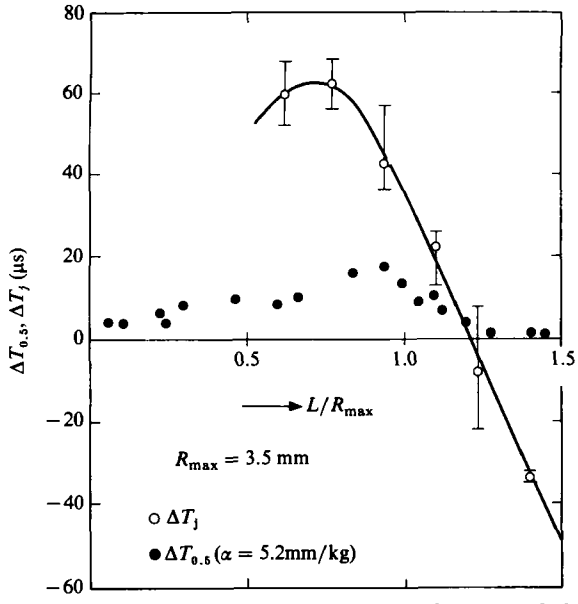

FIGURE 14. Comparison between the initiations of stress fringes and the impact times of liquid jets for various distances L/R_{max}; $R_{max} = 3.5$ mm, $\alpha = 5.2$ mm/kg.

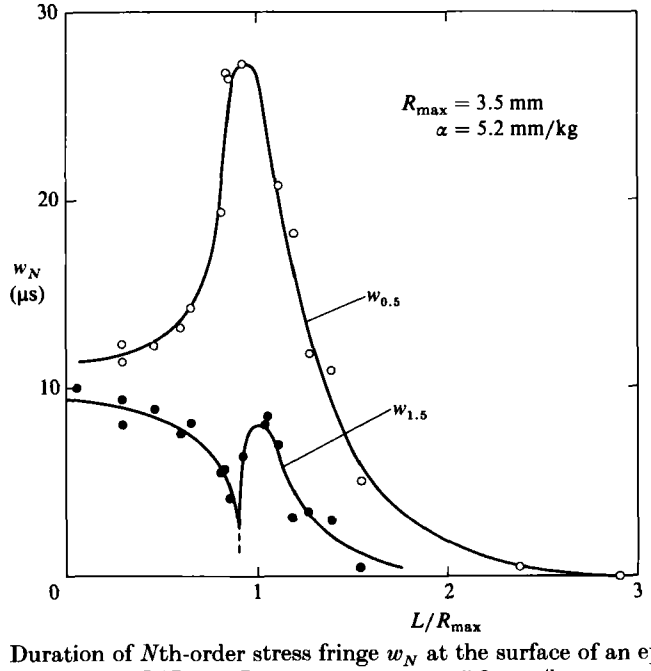

FIGURE 15. Duration of Nth-order stress fringe w_N at the surface of an epoxy plate versus L/R_{max}; $R_{max} = 3.5$ mm, $\alpha = 5.2$ mm/kg.

about 1068 μs, the dimensionless time difference is readily obtained as $\Delta\tau \gtrsim 1.957 \times 10^{-3} \times (1068 - 973) = 0.19$. From figure 6, this value almost corresponds to the impact time of a liquid jet on a solid boundary.

The duration of the fringe at the surface of the epoxy resin is shown in figure 15. As can be seen in figure 13, the shock-wave impact on the surface leads to initiation

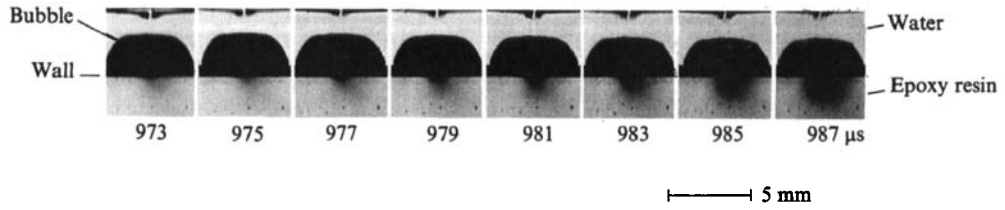

FIGURE 16. Initiation of stress fringe caused by liquid-jet impact; $R_{max} = 5.1$ mm, $L/R_{max} = 0.68$, $\alpha = 5.2$ mm/kg.

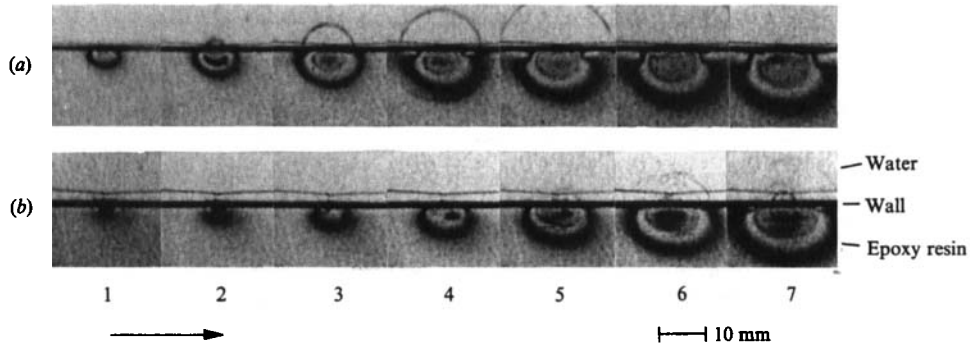

FIGURE 17. Isochromatic fringe patterns in epoxy resins due to impulsive pressure generated at the first collapse of a bubble; (*a*) $L/R_{max} = 0.059$ ($R_{max} = 3.5$ mm); (*b*) $L/R_{max} = 0.43$ ($R_{max} = 5.1$ mm); frame interval 2 μs, exposure 0.4 μs.

of the $\frac{3}{2}$th-order fringe. Since the shape of the $w_{1.5}$ versus L/R_{max} curve is very similar to that of the p_{1max} versus L/R_{max} curve, it can be conjectured that the pressure–time histories measured by the transducer represent the shock-wave pressures. In this connection, an important piece of experimental evidence is the generation of multiple shock waves prior to a main shock wave. It is interesting that the maximum value of $w_{0.5}$ occurs at $L/R_{max} \approx 0.9$, which corresponds exactly to the tendency of plot of the pulse width of pressure wave versus L/R_{max} (Shima *et al.* 1983, 1984).

Figure 17 shows the isochromatic fringe patterns. In particular, an interesting phenomenon can be seen in figure 17(*b*): two longitudinal waves are generated from different points on the model surface. This suggests the generation of local impulsive forces acting on the surface. On the other hand, as shown in figure 8, the solid boundary is probably hit by impulsive pressures at not only the first but also at the second collapse of a bubble near a boundary. Figure 18 shows the fringe patterns for $L/R_{max} = 1.05$ and 0.35. At the second collapse of a bubble, weak stress fringes appear in figure 18(*a*)(2), whereas impulsive stress fringes can be clearly seen in figure 18(*b*)(2). In particular, in the fourth and fifth frames of figure 18(*b*)(2) two fringes can be seen to develop from different portions of the epoxy surface and combine into a single fringe with the passage of time. The new fringe is quite similar to the one at the first collapse shown in figure 18(*a*)(1). In general, a bubble vortex ring composed of a number of tiny bubbles seems to be formed in the torus-like bubble interior after the first collapse of the original bubble. At the second collapse, a part of the ring collapses rapidly and results in the radiation of a shock wave. Lauterborn (1982) observed shock waves emitted from individial tiny bubbles. The pressures caused by the collapse of these bubbles certainly contribute to the fringe initiation in figure 18(*b*)(2).

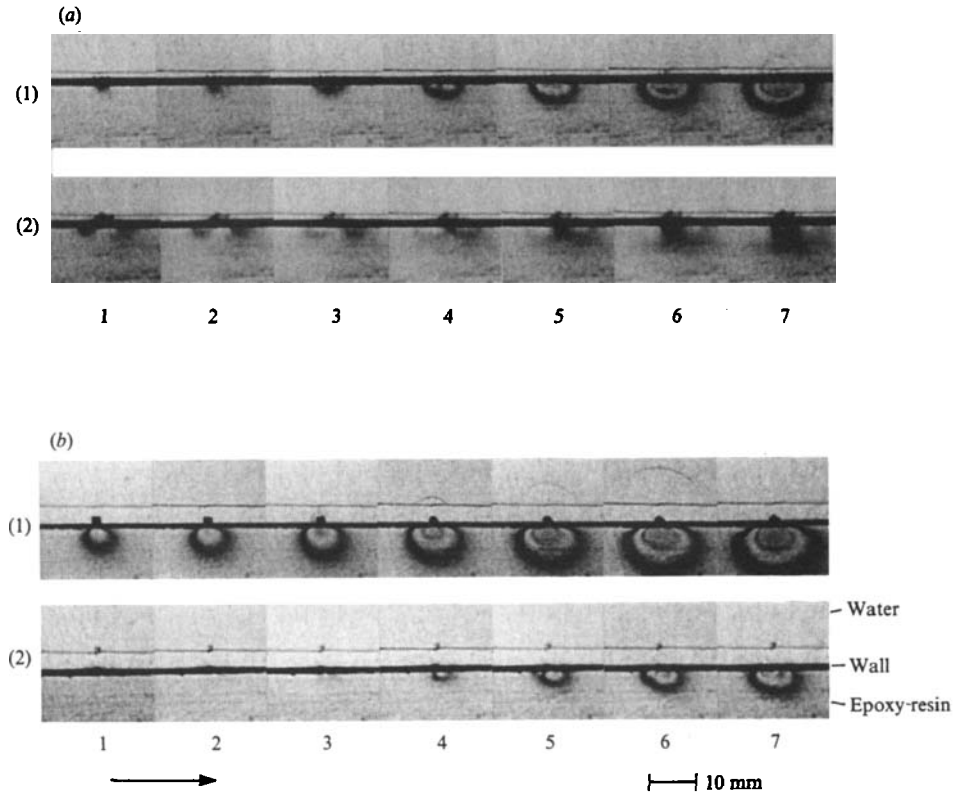

FIGURE 18. Comparison between isochromatic fringe patterns produced at the first and second collapses of a bubble; $R_{max} = 3.5$ mm, $\alpha = 7.3$ mm/kg, frame interval 2 μs, exposure 0.4 μs: (*a*) $L/R_{max} = 0.35$; (*b*) $L/R_{max} = 1.05$; (1) First collapse; (2) second collapse.

3.1.3. *Cause of damage pattern*

The general features of the impulsive pressure have been studied by using a pressure transducer as well as by the photoelastic method. It was found that the impulsive pressure is strongly dependent on the distance of a bubble from a solid boundary. However, the cause of damage is still unknown. To clarify the mechanism of cavitation damage, it is necessary to make precise multiple pressure measurements in both liquid and solid, with high temporal and spatial resolutions. However, there are still several problems to be overcome in doing this.

Another effective method to study the cause of damage – the use of a soft material as a solid boundary – has been applied by several investigators (Naudé & Ellis 1961; Shutler & Mesler 1965; Efimov *et al.* 1976; Singer & Harvey 1979). The method is suitable for registering the damage of material caused by impulsive pressures due to bubble collapse; however, until now, no reasonable interpretation has been made of the relation between the impulsive pressure and the damage pit.

In the following, the cause of damage produced on an indium specimen will be discussed with reference to the results of the photoelastic method. Figure 19 shows the damage patterns caused by spark-induced bubble collapse. The patterns are almost circular. As the distance L from the electrode gap to the indium surface increases (from (*a*) to (*c*) in the figure), the average diameter of the damage pattern D_p increases and its intensity rapidly becomes weaker. As seen before, the solid boundary is subject to various kinds of impulsive pressure produced in bubble

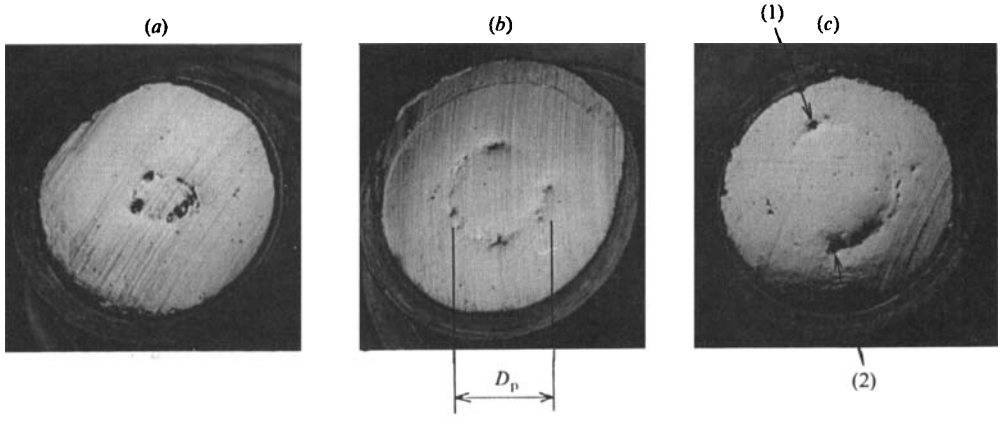

FIGURE 19. Damage patterns produced on indium specimens; $R_{max} = 5.1$ mm: (a) $L/R_{max} = 0.082$; (b) 0.23; (c) 0.32.

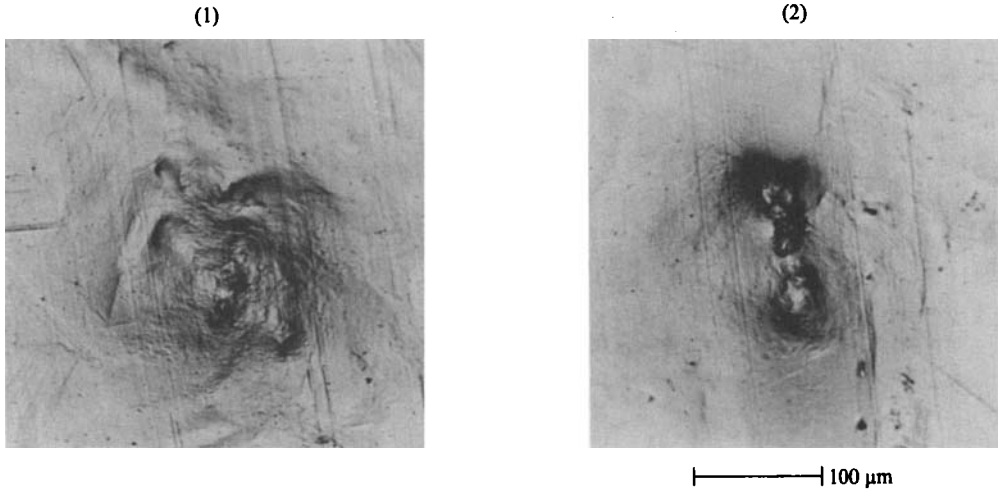

FIGURE 20. Microscopic observations of damage pits indicated in figure 19(c).

collapse: the pressure pulse developed in the liquid near the contracting bubble surface; the impact pressure from a liquid jet; impulsive pressures produced by the interaction between the outward radial flow following jet impact and the contracting bubble surface; and the impact pressure from a shock wave radiated at the rebound of the original bubble. Naudé & Ellis (1961) concluded that the liquid-jet impact is a major cause of damage on the basis of observations that a stress fringe is caused by jet impingement and that damage pits are much smaller than the minimum bubble base diameter. But the cause of damage cannot be judged from only these results. They were confirmed by the present experiment; however, the damage pattern produced on the indium specimen was almost circular, as shown in figure 19. This means that the impulsive pressures caused by both the liquid jet and the shock wave resulting from the collapse of the original bubble scarcely contributed to the permanent deformation of the indium within the limits of the present experiment, and that significantly larger pressures were needed to cause damage on the indium surface.

The circular pattern has been already demonstrated by Shutler & Mesler (1965),

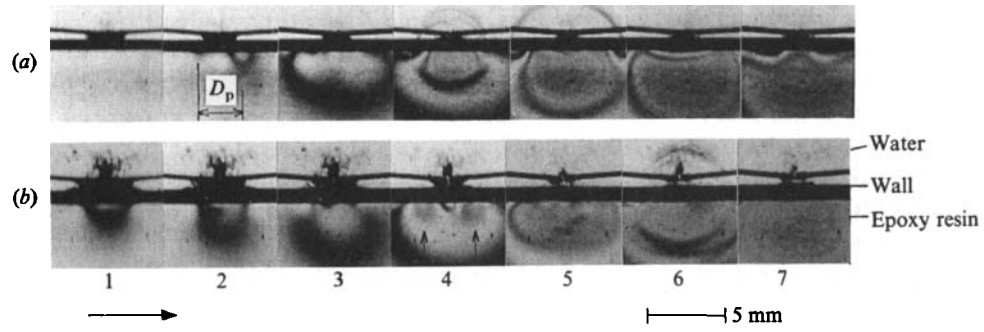

FIGURE 21. Stress fringes generated at the first collapse of a bubble; $\alpha = 5.2$ mm/kg, frame interval 2 μs, exposure 0.4 μs: (*a*) $L/R_{max} = 0.11$ ($R_{max} = 3.5$ mm); (*b*) $L/R_{max} = 0.10$ ($R_{max} = 5.1$ mm).

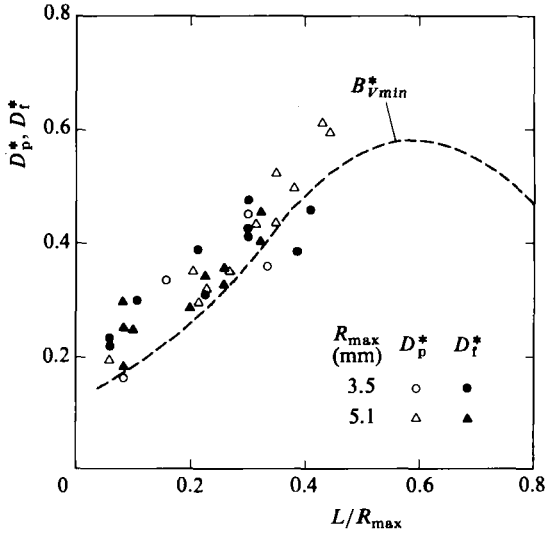

FIGURE 22. Correlation between the initiated fringe diameter D_f^* and the circular pit diameter D_p^*, in which data are normalized by the maximum bubble diameter $2R_{max}$.

who concluded that the damage must be caused by the pressure pulse generated at the minimum volume of a bubble. Since peak pressure is attained in the liquid near the bubble wall during collapse as mentioned above, the circular damage pattern is likely. However, it should be noted that the damaged area on the circumference is not uniform, as shown in figure 19. On observing the damaged surface in detail, it is clear that the circumference consists of shallow depressions and minute pits. The shallow depressions possess exact spherical symmetry.

On the other hand, important experimental evidence has come from the observation of damage pits. Figure 20 shows the detailed structures of the pits marked (1) and (2) in figure 19(*c*), from microscopic observations which were not made by Shutler & Mesler. Double dents can be seen in both cases, and, in particular, minute pits are present around the main pit in (1). The presence of these pits suggest the action of a large number of local impulsive pressures on the circumference. To verify this, the

photoelastic method was used again. Figure 21 shows two typical examples, with a frame interval of 2 μs. Both photographs indicate stress fringes initiated near the contracting bubble surface, where the initial fringe diameter is defined as D_f. In figure 21 (*a*) a small fringe is initiated in the second frame, and a shock wave radiated at the rebound of the original bubble is clearly seen in the fifth frame. Figure 21 (*b*) provides an important piece of evidence in the fourth frame, which shows two smaller fringes indicated by arrows. These smaller fringes are generated at the portion near the contracting bubble surface where the initial fringe occurred. It is reasonable to suppose that tiny bubbles collapse under impulsive pressure, since smaller fringes appear at some time after the occurrence of the initial fringe.

The correlation between the initial fringe diameter D_f^* and the circular-pit diameter D_p^* is examined in figure 22, where data are normalized by the maximum bubble diameter $2R_{max}$. In this figure the broken line indicates the base diameter at minimum bubble volume $B_{V\,min}^*$ (see figure 5). There is good correlation between them. Almost all the data on D_p^* and D_f^* are larger than $B_{V\,min}^*$. This means that the impulsive pressures, which lead to the formation of stress fringes in the final stage of the first collapse of the bubble, result in the circular damage on the indium surface. Consequently the damage pattern produced on the indium must be caused by the impulsive pressures resulting from the collapses of many tiny bubbles. These are formed by the interaction of a contracting bubble surface with the radial flow following liquid-jet impact, and are exposed to the high-pressure field generated in the liquid near the contracting original bubble surface. This mechanism is essentially similar to the energy-transfer model of concerted collapse of clusters of cavities proposed by Hansson & Mørch (1980). For the case of a spark-induced bubble, a liquid jet acts like a tiny bubble generator, while the high pressure developing in the final stage of collapse of an original bubble acts as a driving pressure to collapse individual tiny bubbles. Therefore, it can be taken that the multiple weak shock waves, which appear prior to the shock wave coming from the first rebound of an original bubble, where observed in both photoelastic and schlieren photographs, originate from these tiny bubble collapses. The reason why a high pressure can be produced by the interaction between a tiny bubble and a shock wave (or a pressure wave) will be discussed in the following subsection.

3.2. *Interaction of a gas bubble with a shock wave*

3.2.1. *Possibility of high-pressure generation*

In the preceding subsection it was pointed out that the impulsive pressure contributing to damage is probably produced as a result of the interaction of tiny bubbles with a shock wave or a pressure wave. In connection with the high-pressure generation by the interaction it is necessary to consider the time dependence of the applied pressure around a bubble.

The behaviour of bubbles has frequently been studied assuming a stepwise pressure profile in the liquid (Rayleigh 1917; Hickling & Plesset 1964; Plesset & Chapman 1971; Tomita & Shima 1979; Fujikawa & Akamatsu 1980). In an actual flow field, however, the pressure field around a bubble varies so much with time that it needs to know the time dependence of the impulsive pressure.

We now assume a pressure profile $p_a(t)$ as shown in the insert in figure 23, and investigate the effect of the rise time t_r on the maximum impulsive pressure p_{max}. The function p_a increases linearly with time from zero to t_r and thereafter remains constant, p_∞. Figure 23 shows the result obtained by numerical solution of the following equation under conditions where the ambient pressure at infinity

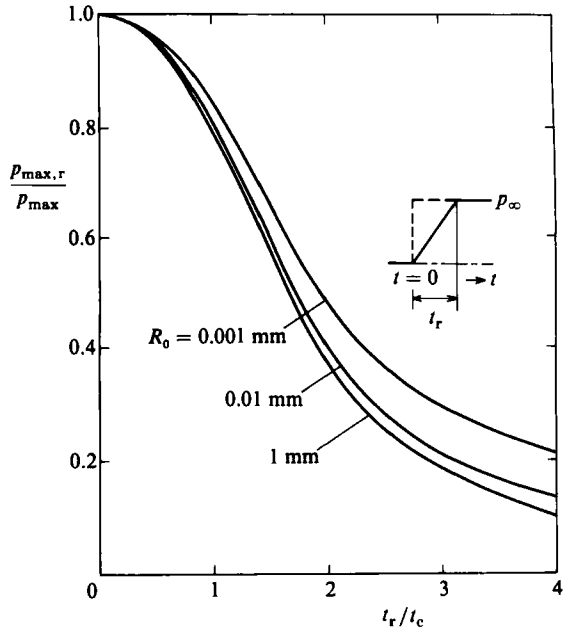

FIGURE 23. Effect of the rise time t_r on the maximum impulsive pressure p_{max} for the pressure profile shown in the insert. The values of $p_{max,0}$ and $t_{c,0}$ correspond to the results for a stepwise pressure profile; $p_\infty = 101.3$ kPa, $T_\infty = 293.2$ K, $p_{g,0}/p_\infty = 0.01$.

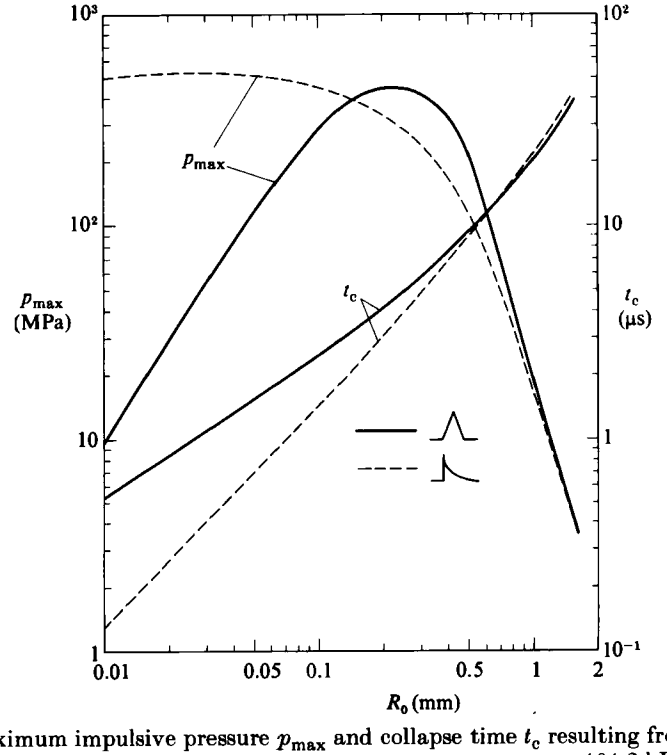

FIGURE 24. Maximum impulsive pressure p_{max} and collapse time t_c resulting from the interaction between a bubble and a shock wave or a pressure wave; $p_\infty = 101.2$ kPa, $T_\infty = 291.5$ K, $F_i = 24.4$ Pa s, $p_s = 5$ MPa.

$p_\infty = 0.1$ MPa and the pressure ratio $p_{g,0}/p_\infty = 0.01$, where $p_{g,0}$ is the initial gas pressure:

$$R\ddot{R}\left(1-\frac{2\dot{R}}{c_\infty}+\frac{23\dot{R}^2}{10c_\infty^2}\right)+\tfrac{3}{2}\dot{R}^2\left(1-\frac{4\dot{R}}{3c_\infty}+\frac{7\dot{R}^2}{5c_\infty^2}\right)+\frac{1}{\rho_\infty}\left[p_a(t)-(p_2)_{r=R}+\frac{R}{c_\infty}(\dot{p}_a-(\dot{p}_1)_{r=R})\right.$$
$$\left.+\frac{1}{c_\infty^2}\left\{-2R\dot{R}(\dot{p}_a-(\dot{p}_1)_{r=R})+\tfrac{1}{2}(p_a-(p_1)_{r=R})\left[\dot{R}^2+\frac{3}{\rho_\infty}(p_a-(p_1)_{r=R})\right]\right\}\right]=0. \quad (5)$$

where

$$(p_1)_{r=R} = p_v+p_{g,0}\left(\frac{R_0}{R}\right)^{3\gamma}-\frac{2\sigma}{R}-\frac{4\mu}{R}\dot{R}, \quad (6)$$

$$(p_2)_{r=R} = (p_1)_{r=R}-\frac{4\mu}{3\rho_\infty c_\infty^2}(\dot{p}_a-(\dot{p}_1)_{r=R}). \quad (7)$$

The detailed derivation of this equation is described in Shima & Tomita (1979) except for the time dependence of the ambient pressure. The result indicates a significant dependence of p_{max} on t_r. For example, p_{max} is smaller than that for the stepwise solution by about 20 % for the case $t_r/t_{c,0} = 1$, and by about 50 % for $t_r/t_{c,0} = 2$, where $t_{c,0}$ is the collapse time of a bubble for the stepwise solution. Since the value of $t_{c,0}$ is about 1 μs when the initial bubble radius $R_0 = 0.01$ mm and about 100 μs when $R_0 = 1$ mm, it is apparent that the collapse of a smaller bubble is not so rapid for an applied pressure with the same rise time.

In contrast, if the applied pressure has a very short rise time but a sufficiently large amplitude, even a tiny bubble can collapse rapidly. Figure 24 shows this case, in which the maximum impulsive pressure p_{max} and the collapse time t_c are plotted against the initial bubble radius R_0. Here a bubble is assumed to be initially in equilibrium at atmospheric pressure and is then collapsed spherically and adiabatically after impingement of a pressure wave with an amplitude of 5 MPa, where the impulse

$$F_t\left(=\int_0^t p\,\mathrm{d}t\right)$$

is 24.4 Pa s. It is found that, for an applied pressure wave with suitable rise time, there is a corresponding optimum bubble size for which the most rapid bubble collapse occurs. This result shows the possibility of high-pressure generation by mutual interaction of a bubble with a shock wave, and suggests that even avalanched bubble collapse is possible in the collapse process of a spark-induced bubble discussed in the preceding subsection.

3.2.2. *Pit formation by interaction of an attached bubble with a shock wave*

In order to make clear the cause of damage by bubble–shock-wave interaction, an experimental study was made. The experiment was mainly focused on the cases where the source of the shock wave is located on the axis of symmetry of a bubble. To collapse an air bubble, a shock wave with amplitude of about 5 MPa was used. It was first noted that in the absence of a gas bubble, the shock-wave impact produced no appreciable damage pit on the indium.

Figure 25 shows some examples of bubble collapse caused by interaction with a shock wave. In each photograph a shock wave impinges on a bubble from vertically

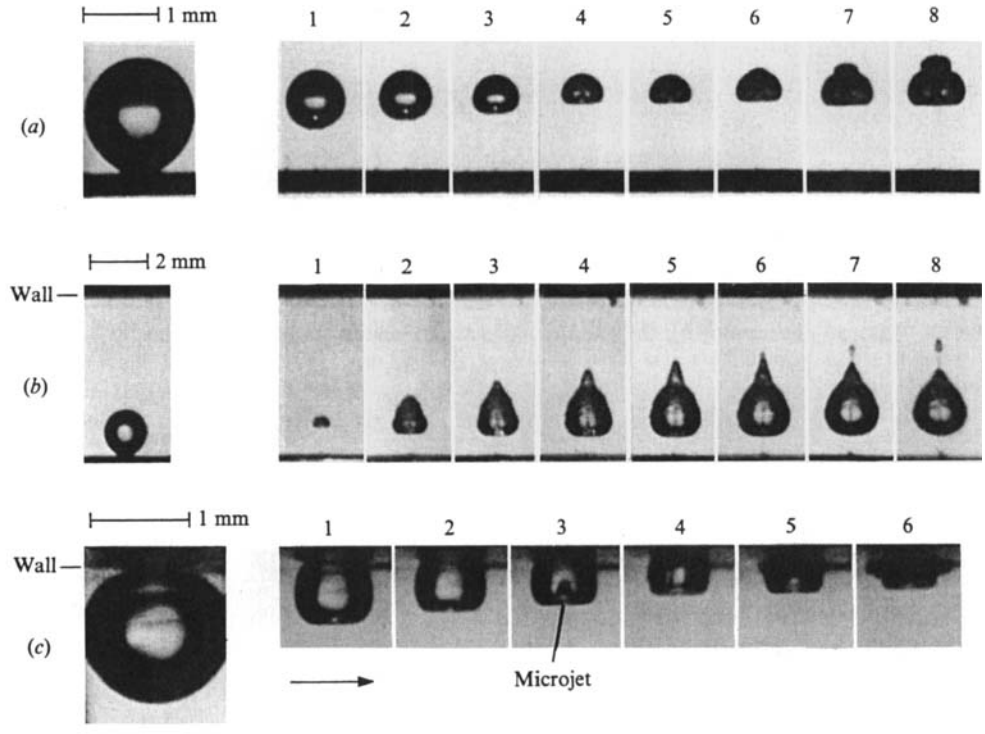

FIGURE 25. Collapse of an air bubble hit by a shock wave: (*a*) $R_e = 0.72$ mm ($l_c/R_e \to \infty$), frame interval 1 μs; (*b*) 0.74 mm ($l_c/R_e = 6.29$), 10 μs; (*c*) 0.77 mm, 1 μs.

below. It should be noted that the bubble–shock-wave interaction leads to liquid-jet formation, even for a bubble in an infinite volume of liquid, owing to the asymmetric flow induced by the shock wave (figure 25*a*). Figure 25(*b*) indicates the bubble behaviour after the first collapse. In the seventh frame it can be seen that the tip of the liquid jet penetrating the bubble interior separates from the original bubble. Figure 25(*c*) shows the case of an attached bubble. The liquid jet is clearly seen, with no disturbance inside the bubble, which is notably different from the case of a spark-induced bubble, where undesirable electrodes are present.

Figure 26 shows damage pits for various sizes of attached bubbles. As seen in figure 26(*a*), the pit is basically made up of a small circular dent at the centre (of diameter $d_{p,c}$) with a dark circle surrounding it (of diameter $d_{p,M}$). The characteristics of the pit depend on the intensity of the bubble collapse, which is closely related to the bubble size for a constant shock strength. An intensive damage pit accompanying cracks with slip lines at its rim is produced when the bubble size is close to the optimum one as shown in figure 24. To make clear the cause of these pits, simultaneous measurements of bubble collapse and the subsequent damage pit were carried out. The results are shown in figures 27 and 28 in which photographs were taken with a framing rate of 2×10^6 frames/s. In each photograph a separate frame at the left-hand corner indicates the initial stationary state of the bubble. The bubble is hit by a shock wave from below and begins to collapse. From figure 27 it is obvious that the bubble configuration is cylindrical rather than hemispherical in the final stage of collapse, where the bubble size often satisfies the condition $R/R_0 < 0.2$. Therefore the jet size appearing in the photograph is probably close to the actual one. The

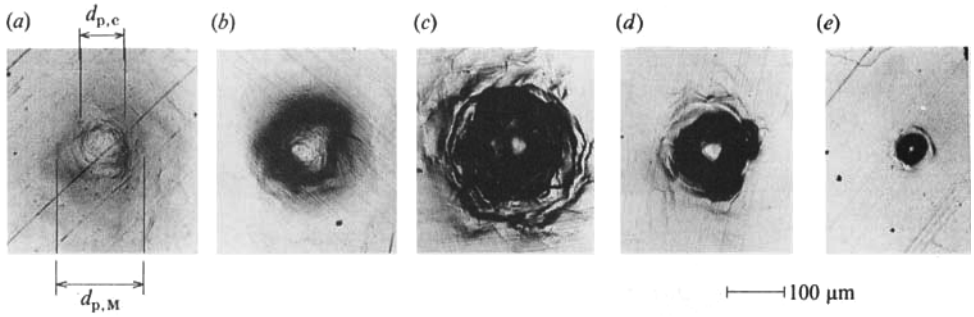

FIGURE 26. Damage pits caused by the collapses of various sizes of bubbles; the amplitude of the shock-wave pressure $p_s = 5$ MPa: (*a*) $R_e = 0.64$ mm; (*b*) 0.43 mm; (*c*) 0.32 mm; (*d*) 0.25 mm; (*e*) 0.10 mm.

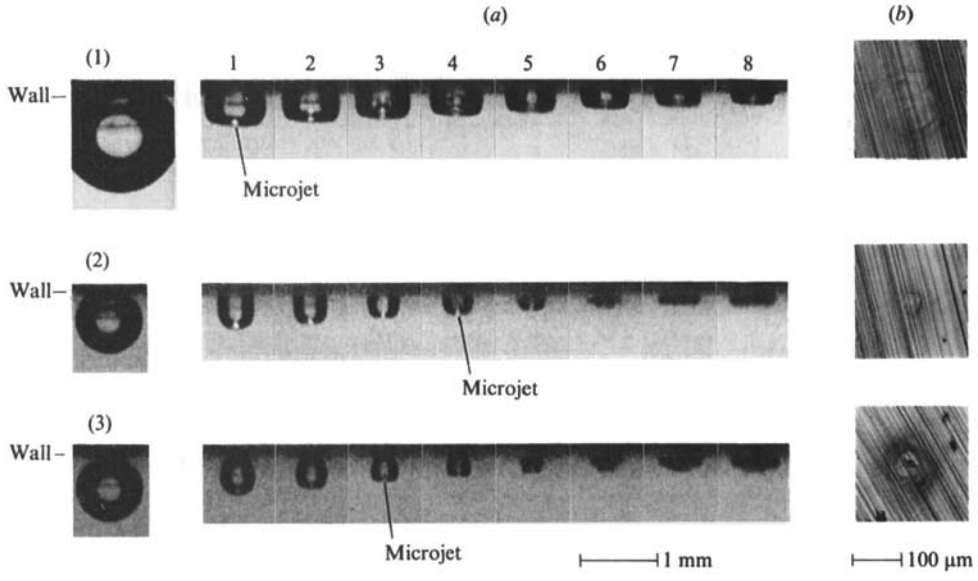

FIGURE 27. Collapse of an attached air bubble by a shock wave and subsequent damage pit (1): (*a*) collapse process of a bubble; frame interval 0.5 μs, exposure 0.1 μs; (*b*) damage pits. (1) $R_e = 0.78$ mm; (2) 0.42 mm; (3) 0.42 mm.

configuration of the liquid jet formed within a bubble is nearly conical, with a slightly rounded nose following straight part with moderate taper. $d'_{j,c}$ and $d'_{j,M}$ are respectively the jet diameters at the origin and the end of the straight part. In figure 27 the pictures (2) and (3) are of bubbles with identical equivalent radii $R_e = 0.42$ mm, but with different adherent conditions. Comparing damage pits for the two cases, it is found that the pit in (3) is larger than that in (2) owing to the adherent effect of the bubble. On the other hand, in figure 28, (2) and (3) are bubbles in contact with the indium surface, and (1) is a nearly hemispherical bubble. Multiple shock waves are radiated into the water in cases (2) and (3), whereas a hemispheriel shock wave can be seen in (1). Although the shock wave in (1) is clearer than that in (2) the pit in the former is apparently weaker than in the latter. This suggests that it is difficult to relate the damage strength to the schlieren image. In figure 28 (3) a larger damage

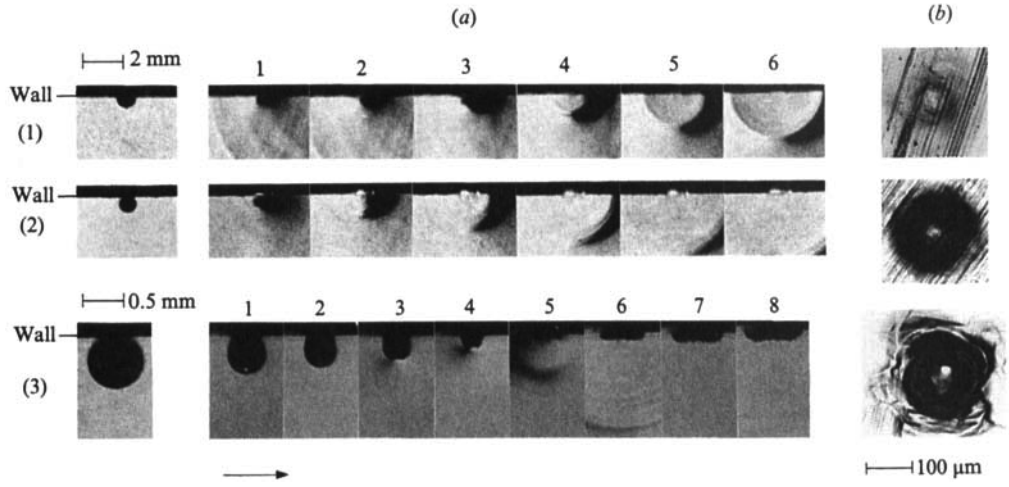

FIGURE 28. Collapse of an attached air bubble by a shock wave and subsequent damage pit (2): (*a*) collapse process of a bubble; frame interval 0.5 μs. exposure 0.1 μs; (*b*) damage pit. (1) $R_e = 0.45$ mm; (2) 0.42 mm; (3) 0.32 mm.

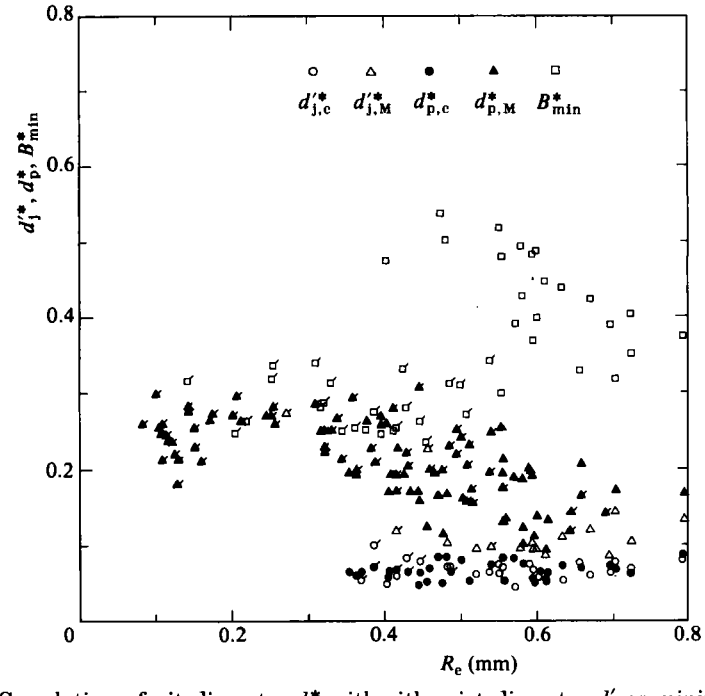

FIGURE 29. Correlation of pit diameter d^*_p with either jet diameter d'_j or minimum bubble base diameter B^*_{min}, where all data are normalized by the diameter of the equivalent sphere having the same volume as the attached air bubble; $p_s = 5$ MPa.

pit with cracks and slip lines is caused by rapid collapse of a bubble with radius $R_e = 0.32$ mm, which is close to the optimum bubble size when $p_s = 5$ MPa.

Results normalized by the diameter of an equivalent sphere are shown in figure 29. Here B^*_{min} is the dimensionless minimum bubble base diameter, and the data with bar denote results for bubbles almost in contact with the indium surface. The good

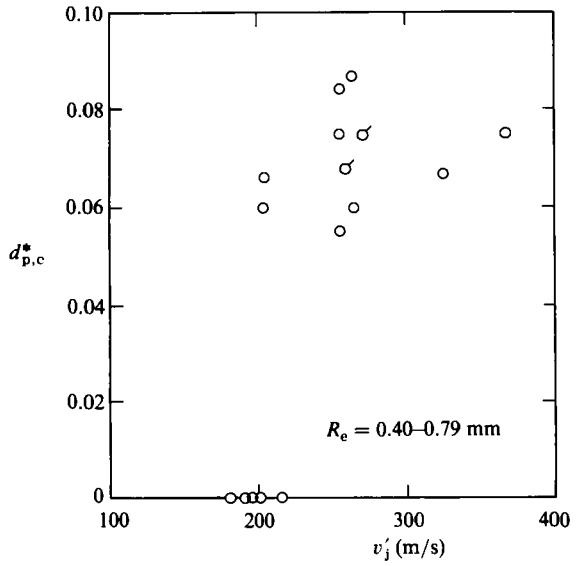

FIGURE 30. Threshold value of impact velocity of a liquid jet for causing a damage pit.

correlation between $d^*_{p,c}$ and $d'^*_{j,c}$ is obvious, so that the smaller circular dent at the centre of the damage pit must be caused by the impulsive pressure resulting from the liquid-jet impact. An average value of $d'^*_{j,c}$ is given as 0.07, independently of the bubble radius R_e. This value agrees reasonably with the previous result (Plesset & Chapman 1971). The configuration of the damage pit, like a circular dent, as seen in figure 27, is the results of the three-dimensional structure of a liquid jet whose behaviour is approximately analogous to that of a conical water drop, which was solved numerically by Hwang & Hammitt (1977). They obtained the important result that the greatest pressure on the solid surface is produced on the ring with diameter almost equivalent to the jet diameter $d'_{j,c}$, and its value is larger than that of the water-hammer pressure corresponding to the impact velocity. A similar phenomenon will occur with a liquid jet formed within a bubble.

As shown in figure 30, in the present experiment, a virtual jet velocity of over 200 m/s is needed to cause an appreciable damage pit (i.e. more than 1–2 μm in depth) on the indium surface. The water-hammer pressure corresponding to this value exceeds 300 MPa, which is more than ten times the yield point of indium. The duration of this pressure can be estimated from (4) to be 10^{-8}–10^{-7} s for a bubble with radius of about 0.3–0.8 mm. When material is hit by such an impulsive pressure, plastic deformation probably occurs at the dynamic level, which is situated in a stress state higher than that of the so-called yield point. Generally, plastic deformation depends on the amount of dislocation. For impulsive pressure with very short duration, however, there is less time for dislocations to grow, so that significantly larger pressure is needed to deform a material. On the other hand, the cause of $d^*_{p,M}$ is still an open question; however, $d^*_{p,M}$ seems to be correlated with $d'^*_{j,M}$ for larger R_e and with B^*_{min} for smaller R_e.

Finally, we examine an additional case, where an attached bubble is hit by a shock wave from an oblique direction different from the axis of symmetry of the bubble. Figure 31 shows a typical result for this case. The bubble surface is deformed from the side hit by the shock wave, and subsequently an oblique liquid jet is formed inside

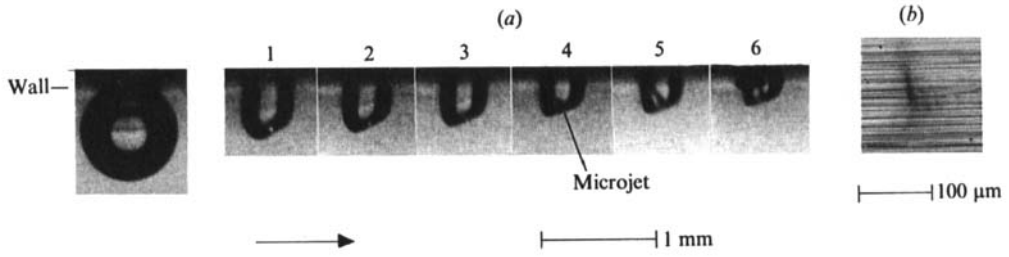

FIGURE 31. Collapse of an attached air bubble by a shock wave from an oblique direction different from the axis of symmetry of the bubble and subsequent damage pit; $R_e = 0.41$ mm, frame interval 0.5 μs, exposure 0.1 μs.

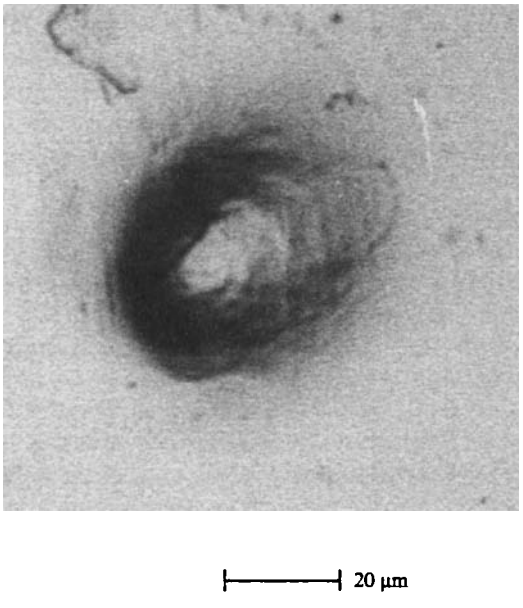

FIGURE 32. Damage pit caused by the impact of an oblique liquid jet formed within a bubble; $R_e = 0.11$ mm.

the bubble. The jet impacts on the indium surface and then spreads outward. The damaged surface in this occasion is very different from that described before. Since the width of this damage agrees fairly well with the liquid-jet diameter, there is no doubt that the asymmetric damage pit must be caused by the impact of the oblique jet. The deformation of the indium surface proceeds asymmetrically because of instantaneous compressible and shear forces. Figure 32 shows another typical example of pits. Damage of this type can be artificially imitated with a bar pushing on a plasticine surface from an oblique direction. The problem of bubble–shock-wave interaction has been further studied by Tomita *et al.* (1986), who also presented results on the damage to an indium surface exposed to vibratory cavitation. The impacts of an oblique liquid jet on the boundary occur frequently, since many asymmetric effects are present in actual cavitating flows.

4. Conclusions

A detailed experimental study has been made in order to clarify the mechanisms of impulsive pressure generation and damage-pit formation by bubble collapse. Consequently the following conclusions have been reached.

(i) The modes of bubble collapse are dependent on the proximity to a boundary. At the first collapse of a bubble that is either very close to or attached to a boundary (both of which are important situations in relation to cavitation damage) the following impulsive pressures occur in an extremely short duration: (1) the pressure pulse during bubble collapse; (2) the impact pressure from a liquid jet formed within the original bubble; (3) impulsive pressures caused by collapses of many tiny bubbles resulting from the interaction between the outward radial flow following liquid-jet impact and the contracting bubble surface; and (4) the impact pressure from a shock wave radiated from the torus-like original bubble at its rebound.

(ii) In particular, for a bubble situated very close to a solid boundary, intensive impulsive pressures occur not only at the first collapse but also at the second collapse of a bubble. The latter may result from the collapse of individual tiny bubbles formed through the collapse process of the original bubble. On this occasion, the bubble–shock-wave interactions contributes to the generation of locally high impulsive pressure.

(iii) The circular damage pattern on indium caused by spark-induced bubble collapse results from the impulsive pressures mentioned in (i)(3). The individual pits formed on the circumference seem to be caused by the collapses of induced tiny bubbles.

(iv) Local high pressure may occur as a result of the interaction of a tiny bubble with either a shock wave or a pressure wave with a sufficiently large amplitude and sharp rise time. For a pressure pulse with a constant amplitude and duration, there is an optimum size for which the most rapid bubble collapse can occur.

(v) The damage pit was caused by the interaction of an attached air bubble with a shock wave. In this case, the pit formation results from the impact pressure of a liquid microjet. Additional impulsive pressures immediately before and after the impingement of the jet, as mentioned in (i), increase the deformation of indium. The fact that these impulsive pressures successively impinge on the surface in a short duration is of primary significance in causing material deformation.

(vi) When an attached bubble is hit by a shock wave from a direction different to the axis of symmetry of the bubble, the subsequent damage pit exhibits a remarkable feature due to the impact of an oblique liquid jet. The occurrence of this asymmetric pit was limited to a narrow region in the neighbourhood of the optimum bubble size.

The authors wish to express their thanks to Professor K. Takayama of Tohoku University for his useful suggestions in this work. Assistance received from Mr N. Miura, Mr K. Shoji and Miss M. Sekii is acknowledged with thanks. The present project was financially supported by the Science and Research Grant in Aid from the Ministry of Education of Japan in 1984.

REFERENCES

BENJAMIN, T. B. & ELLIS, A. T. 1966 The collapse of cavitation bubbles and the pressures thereby produced against solid boundaries. *Phil. Trans. R. Soc. Lond.* A **260**, 221–240.

BOWDEN, F. P. & BRUNTON, J. H. 1961 The deformation of solids by liquid impact at supersonic speeds. *Proc. R. Soc. Lond.* A **263**, 433–450.

EFIMOV, A. V., VOROBEV, G. A., FILENKO, YU. I. & PETROV, K. N. 1976 Mechanism of cavitation damage and structure of a cavitating eddy. In *Proc. IAHR Symp. on Two-Phase Flow and Cavitation in Energy Production Systems, Grenoble*, pp. 159–169.

FUJIKAWA, S. & AKAMATSU, T. 1978 Experimental investigations of cavitation bubble collapse by a water shock tube. *Bull. Japan Soc. Mech. Eng.* **21**, 223–230.

FUJIKAWA, S. & AKAMATSU, T. 1980 Effects of the non-equilibrium condensation of vapour on the pressure wave produced by the collapse of a bubble in a liquid. *J. Fluid Mech.* **97**, 481–512.

GIBSON, D. C. 1968 Cavitation adjacent to plane boundaries. In *Proc. 3rd Australasian Conf. on Hydraulics and Fluid Mechanics, Institution of Engineers, Sydney*, pp. 210–214.

HANSSON, I. & MØRCH, K. A. 1980 The dynamics of cavity clusters in ultrasonic (vibratory) cavitation erosion. *J. Appl. Phys.* **51**, 4651–4658.

HICKLING, R. & PLESSET, M. S. 1964 Collapse and rebound of a spherical bubble in water. *Phys. Fluids* **7**, 7–14.

HUANG, Y. C., HAMMITT, F. G. & YANG, W.-J. 1973 Hydrodynamic phenomena during high-speed collision between liquid droplet and rigid plane. *Trans. ASME* I: *J. Fluids Engng* **95**, 276–294.

HWANG, J.-B. G. & HAMMITT, F. G. 1977 High-speed impact between curved liquid surface and rigid flat surface. *Trans. ASME* I: *J. Fluids Engng* **99**, 396–404.

KLING, C. L. & HAMMITT, F. G. 1972 A photographic study of spark-induced cavitation bubble collapse. *Trans. ASME* D: *J. Basic Engng* **94**, 825–833.

KNAPP, R. T. 1955 Recent investigations of the mechanics of cavitation and cavitation damage. *Trans. ASME* **77**, 1045–1054.

KORNFELD, M. & SUVOROV, L. 1944 On the destructive action of cavitation. *J. Appl. Phys.* **15**, 495–506.

LAUTERBORN, W. 1982 Cavitation bubble dynamics – new tools for an intricate problem. *Appl. Sci. Res.* **38**, 165–178.

LAUTERBORN, W. & BOLLE, H. 1975 Experimental investigation of cavitation-bubble collapse in neighbourhood of a solid boundary. *J. Fluid Mech.* **72**, 391–399.

NAUDÉ, C. F. & ELLIS, A. T. 1961 On the mechanism of cavitation damage by nonhemispherical cavities collapsing in contact with a solid boundary. *Trans. ASME* D: *J. Basic Engng* **83**, 648–656.

PLESSET, M. S. & CHAPMAN, R. B. 1971 Collapse of an initially spherical vapour cavity in the neighbourhood of a solid boundary. *J. Fluid Mech.* **47**, 283–290.

RAYLEIGH, LORD 1917 On the pressure developed in a liquid during the collapse of a spherical cavity. *Phil. Mag.* **34**, 94–98.

SHIMA, A., TAKAYAMA, K. & TOMITA, Y. 1984 Mechanisms of the bubble collapse near a solid wall and the induced impact pressure generation. *Rep. Inst. High Speed Mech., Tohoku Univ.* **48**, 77–97.

SHIMA, A., TAKAYAMA, K., TOMITA, Y. & MIURA, N. 1981 An experimental study on effects of a solid wall on the motion of bubbles and shock waves in bubble collapse. *Acustica* **48**, 293–301.

SHIMA, A., TAKAYAMA, K., TOMITA, Y. & OHSAWA, N. 1983 Mechanism of impact pressure generation from spark-generated bubble collapse near a wall. *AIAA J.* **21**, 55–59.

SHIMA, A. & TOMITA, Y. 1979 The behavior of a spherical bubble in mercury. Report 2. *Rep. Inst. High Speed Mech., Tohoku Univ.* **39**, 19–45.

SHIMA, A., TOMITA, Y. & TAKAHASHI, K. 1984 The collapse of a gas bubble near a solid wall by a shock wave and the induced impulsive pressure. *Proc. Instn Mech. Engrs* **198C**, 81–86.

SHUTLER, N. D. & MESLER, R. B. 1965 A photographic study of the dynamics and damage capabilities of bubbles collapsing near solid boundaries. *Trans. ASME* D: *J. Basic Engng* **87**, 648–656.

SINGER, B. G. & HARVEY, S. J. 1979 Cavitation damage studies using plasticine. *Int. J. Mech. Sci.* **21**, 409–416.

TOMITA, Y. & SHIMA, A. 1979 The effects of heat transfer on the behavior of a bubble and the impulse pressure in a viscous compressible liquid. *Z. angew. Math. Mech.* **59**, 297–306.

TOMITA, Y., SHIMA, A. & OHNO, T. 1984 Collapse of multiple gas bubbles by a shock wave and induced impulsive pressure. *J. Appl. Phys.* **56**, 125–131.

TOMITA, Y., SHIMA, A. & SUGIU, T. 1986 Mechanisms of impulsive pressure generation and damage pit formation by bubble–shock wave interaction. In *Proc. Intl Symp. on Cavitation, Sendai*, (ed. H. Murai), pp. 77–82.

TOMITA, Y., SHIMA, A. & TAKAHASHI, K. 1983 The collapse of a gas bubble attached to a solid wall by a shock wave and the induced impact pressure. *Trans. ASME* I: *J. Fluids Engng* **105**, 341–349.

TULIN, M. P. 1969 On the creation of ultra-jets. In *L. I. Sedov 60th Anniversity Volume*: *Problems of Hydrodynamics and Continuum Mechanics*, pp. 725–747. Society for Industrial and Applied Mathematics, Philadelphia.